FORENSIC FACIAL RECONSTRUCTION USING MESH TEMPLATE DEFORMATION WITH DETAIL TRANSFER OVER HRBF

Rafael Oliveira Romeiro

Dissertação de Mestrado apresentada ao Programa de Pós-graduação em Engenharia de Sistemas e Computação, COPPE, da Universidade Federal do Rio de Janeiro, como parte dos requisitos necessários à obtenção do título de Mestre em Engenharia de Sistemas e Computação.

Orientador: Ricardo Guerra Marroquim

Rio de Janeiro
Maio de 2014

FORENSIC FACIAL RECONSTRUCTION USING MESH TEMPLATE DEFORMATION WITH DETAIL TRANSFER OVER HRBF

Rafael Oliveira Romeiro

DISSERTAÇÃO SUBMETIDA AO CORPO DOCENTE DO INSTITUTO ALBERTO LUIZ COIMBRA DE PÓS-GRADUAÇÃO E PESQUISA DE ENGENHARIA (COPPE) DA UNIVERSIDADE FEDERAL DO RIO DE JANEIRO COMO PARTE DOS REQUISITOS NECESSÁRIOS PARA A OBTENÇÃO DO GRAU DE MESTRE EM CIÊNCIAS EM ENGENHARIA DE SISTEMAS E COMPUTAÇÃO.

Examinada por:

Prof. Ricardo Guerra Marroquim, D.Sc.

Prof. Claudio Esperança, Ph.D.

Prof. Cristina Nader Vasconcelos, D.Sc.

RIO DE JANEIRO, RJ – BRASIL
MAIO DE 2014

Romeiro, Rafael Oliveira

Forensic Facial Reconstruction using Mesh Template Deformation with Detail Transfer over HRBF/Rafael Oliveira Romeiro. – Rio de Janeiro: UFRJ/COPPE, 2014.

XI, 45 p.: il.; 29, 7cm.

Orientador: Ricardo Guerra Marroquim

Dissertação (mestrado) – UFRJ/COPPE/Programa de Engenharia de Sistemas e Computação, 2014.

Bibliography: p. 37 – 40.

1. facial reconstruction. 2. hrbf. 3. detail transfer. I. Marroquim, Ricardo Guerra. II. Universidade Federal do Rio de Janeiro, COPPE, Programa de Engenharia de Sistemas e Computação. III. Título.

Agradecimentos

Gostaria de agradecer, primeiramente, à minha família por todo o apoio ao longo desses anos.

À minha namorada, Nayara, pelo enorme carinho.

Ao professor Ricardo Marroquim, por ter me orientado neste trabalho e ter tido paciência com minhas eventuais ausências.

À Andreia Breda, por ter me dado a inesperada oportunidade de participar nesta colaboração tão valiosa e agradável, que espero que continue além deste trabalho.

Também gostaria de agradecer ao Marcos Paulo e ao Santa Martha por terem aceitado participar de nossos testes.

Ao professor Claudio Esperança, por me fornecer a biblioteca de MLS e pelos pitacos experientes.

Ao Emilio Brazil, por me fornecer a biblioteca de HRBF, por todo o amparo matemático e, principalmente, pela oportunidade de estar indo agora fazer pesquisa no Canadá.

A todos os amigos e aos colegas de laboratório que contribuíram, direta ou indiretamente, na realização deste trabalho.

Resumo da Dissertação apresentada à COPPE/UFRJ como parte dos requisitos necessários para a obtenção do grau de Mestre em Ciências (M.Sc.)

RECONSTRUÇÃO FACIAL FORENSE UTILIZANDO DEFORMAÇÃO DE *TEMPLATE* COM TRANSFERÊNCIA DE DETALHE SOBRE HRBF

Rafael Oliveira Romeiro

Maio/2014

Orientador: Ricardo Guerra Marroquim

Programa: Engenharia de Sistemas e Computação

Reconstrução facial forense é a aplicação de antropologia, arte e ciência forense para recriar a face de um indivíduo a partir de seu crânio. Geralmente, é feita manualmente com barro por um escultor e é considerada uma técnica subjetiva, pois depende de uma interpretação artística das características do crânio. Neste trabalho, propomos um método computadorizado baseado em regras anatômicas que sistematicamente gera a superfície da face através de um procedimento de deformação baseada em HRBF sobre um modelo em malha. Nossas principais contribuições são um conjunto mais amplo de regras anatômicas a ser aplicadas sobre as estruturas de tecido mole e um novo método de deformação que dissocia os detalhes do formato geral do modelo.

Abstract of Dissertation presented to COPPE/UFRJ as a partial fulfillment of the requirements for the degree of Master of Science (M.Sc.)

FORENSIC FACIAL RECONSTRUCTION USING MESH TEMPLATE DEFORMATION WITH DETAIL TRANSFER OVER HRBF

Rafael Oliveira Romeiro

May/2014

Advisor: Ricardo Guerra Marroquim

Department: Systems Engineering and Computer Science

Forensic facial reconstruction is the application of anthropology, art and forensic science to recreate the face of an individual from his skull. It is usually done manually by a sculptor with clay and is considered a subjective technique as it relies upon an artistic interpretation of the skull features. In this work, we propose a computerized method based on anatomical rules that systematically generates the surface of the face through a HRBF deformation procedure over a mesh template. Our main contributions are a broader set of anatomical rules being applied over the soft tissue structures and a new deformation method that dissociates the details from the overall shape of the model.

Contents

List of Figures **ix**

List of Tables **xi**

1 Introduction **1**
1.1 Technique overview 2

2 Related work **4**

3 Craniometric points restriction **7**

4 Curves restriction **13**

5 Anatomical restrictions **15**
5.1 Nose 15
5.1.1 Nasal profile 15
5.1.2 Nasal width 17
5.1.3 Nasal tip curve 18
5.2 Eyes 18
5.2.1 Eyeball and canthi positions 18
5.2.2 Palpebral margins 19
5.3 Mouth 19
5.3.1 Mouth fissure and lip thickness 19
5.3.2 Mouth width 21
5.3.3 Cupid's bow 21
5.4 Ears 21
5.5 Reconstruction configuration 23

6 Template restrictions **25**

7 Results **28**

8 Conclusion and future works **35**

Bibliography **37**

A Hermitian Radial Basis Function **41**

A.1 Function approximation with RBF 41

A.2 Surface approximation with RBF 42

A.3 Functional analysis 42

A.4 First-order Hermite interpolation with RBF 43

List of Figures

1.1 Complete workflow of our method: (a) The target HRBF is created from the craniometric points, skin thickness and anatomical rules; (b) The origin HRBF is created from the template; (c) The detail displacement vectors are created from the differences between the template and the origin HRBF; (d) The face reconstruction is obtained by adding the detail displacement vectors to the target HRBF. 3

3.1 Anatomical planes: Frankfurt plane (blue), Midsagittal plane (red) and Coronal plane (green) 9
3.2 Circular and elliptical normal direction adjustments 9
3.3 Craniometric points restriction 10
3.4 Craniometric points restriction with direction adjustment 10
3.5 Craniometric point positions in frontal view and side view 12

4.1 Curves restriction 13

5.1 Pronasale and subspinale computation 16
5.2 The two tangents method 16
5.3 Prokopec and Ubelaker nose profile method 16
5.4 Nasal width 17
5.5 Nasal tip curve 18
5.6 Eyeball and canthi positions 19
5.7 Palpebral margins 20
5.8 Mouth craniometric measurements 20
5.9 Mouth prediction 21
5.10 Cupid's bow 22
5.11 Ear measurements 22

6.1 Reconstruction with nose mesh restriction 25
6.2 HRBF face approximation for detail transfer 27
6.3 The detail (black) over the smooth HRBF surface (grey) being transferred to the other smooth HRBF surface 27

7.1 Different nasal width methodologies 29
7.2 Different nasal profile methodologies 29
7.3 Different nasal tip curve methodologies 30
7.4 Different mouth width methodologies 30
7.5 Template, deformations and scanned face comparison for caucasoid male 31
7.6 Template, deformations and scanned face comparison for caucasoid female 31
7.7 Template, deformations and scanned face comparison for negroid male 31
7.8 Reconstructions of all the combinations of test subject skulls and templates 32
7.9 Ethnicity limitation 33
7.10 Final facial reconstruction (blue) and scanned face (red) for the caucasoid male test subject 33
7.11 Final facial reconstruction (blue) and scanned face (red) for the caucasoid female test subject 34
7.12 Final facial reconstruction (blue) and scanned face (red) for the negroid male test subject 34

8.1 Caucasoid template (Figure 7.5a) deformed for the caucasoid male test subject (Figure 7.5d) with detail transfer over HRBF without anatomical rules. It still meets the craniometric constraints perfectly 36

List of Tables

3.1 Summary of the skin thickness and normal direction adjustment used for craniometric points 11

5.1 Linear regressions for the nasal profile 15
5.2 Nasal width formulas 17
5.3 Eye proportions 19
5.4 Mouth formulas 22
5.5 Ear average values 22
5.6 Summary of the reconstruction options 23
5.7 Summary of the craniometric points used 24

Chapter 1

Introduction

In forensic science, human skeletal remains may be identified with methods of high accuracy like DNA analysis or comparison with antemortem dental records. Sometimes, these traditional means of identification may not be possible or practical due to several reasons (lack of antemortem information, edentulousness, condition of the remains, cost etc). In these cases, facial reconstruction can be used as a last resort for positive identification or to narrow the search field.

In traditional facial reconstruction the first step is the addition of markers to indicate the depth of the tissue at specific points (craniometric points) over a skull or skull replica. The tissue depth data is usually obtained from a lookup table defined from previous studies and based on ancestry, gender and age. The muscles are then modeled with clay following anatomical guidelines regarding their origins and insertions. Finally, the skull is filled with clay until all the depth markers have been covered. In this process, the face morphology is determined by the artist employing different standards related to the facial features [1]. Methodologies using digital models usually rely on the same manual process using 3D modeling tools.

The traditional methodologies (manual or digital) are very time consuming and are prone to artistic subjectivity, whereas an automatic computer methodology can be performed in just a few minutes with reproducible deterministic results. The main challenge regarding automatic methodologies is the adaptation of the traditional guidelines to be applied in an automatic manner inside a geometrically accurate environment.

Our goal in this work is to produce automatic facial reconstructions with all the soft tissue structures without being biased toward predefined templates.

Contributions The contributions of this work are twofold. First, we adapt a broad set of anatomical rules, giving them strict geometric interpretation so that they can be computed and simultaneously applied. Second, we propose a template deformation method that takes into account all the anatomical rules over the soft

tissue structures while suiting them to the overall shape of the skull.

In addition, by allowing a combination of different methodologies, this works also contributes as a validation tool for the techniques from the facial reconstruction literature, since it is deterministic and thus free from human interpretation.

1.1 Technique overview

Our method begins with the manual identification of the craniometric points on the skull. Then, the predefined thickness of soft tissue for each craniometric point is used in conjunction with the normals obtained from the skull model to produce an initial set of target face points. This set is increased with more points as each anatomical rule is applied. When all the desired anatomical rules have been used, the final set of target face points is achieved. For each point in the set of target face points, there is a corresponding origin point in the template face model. A HRBF surface is created from the set of target face points and another from the set of origin template points. The differences between the template and the HRBF surface created from the set of origin template points are then added to the HRBF surface created from the set of target face points, thus yielding the final result of the facial reconstruction. The whole process is illustrated in Figure 1.1.

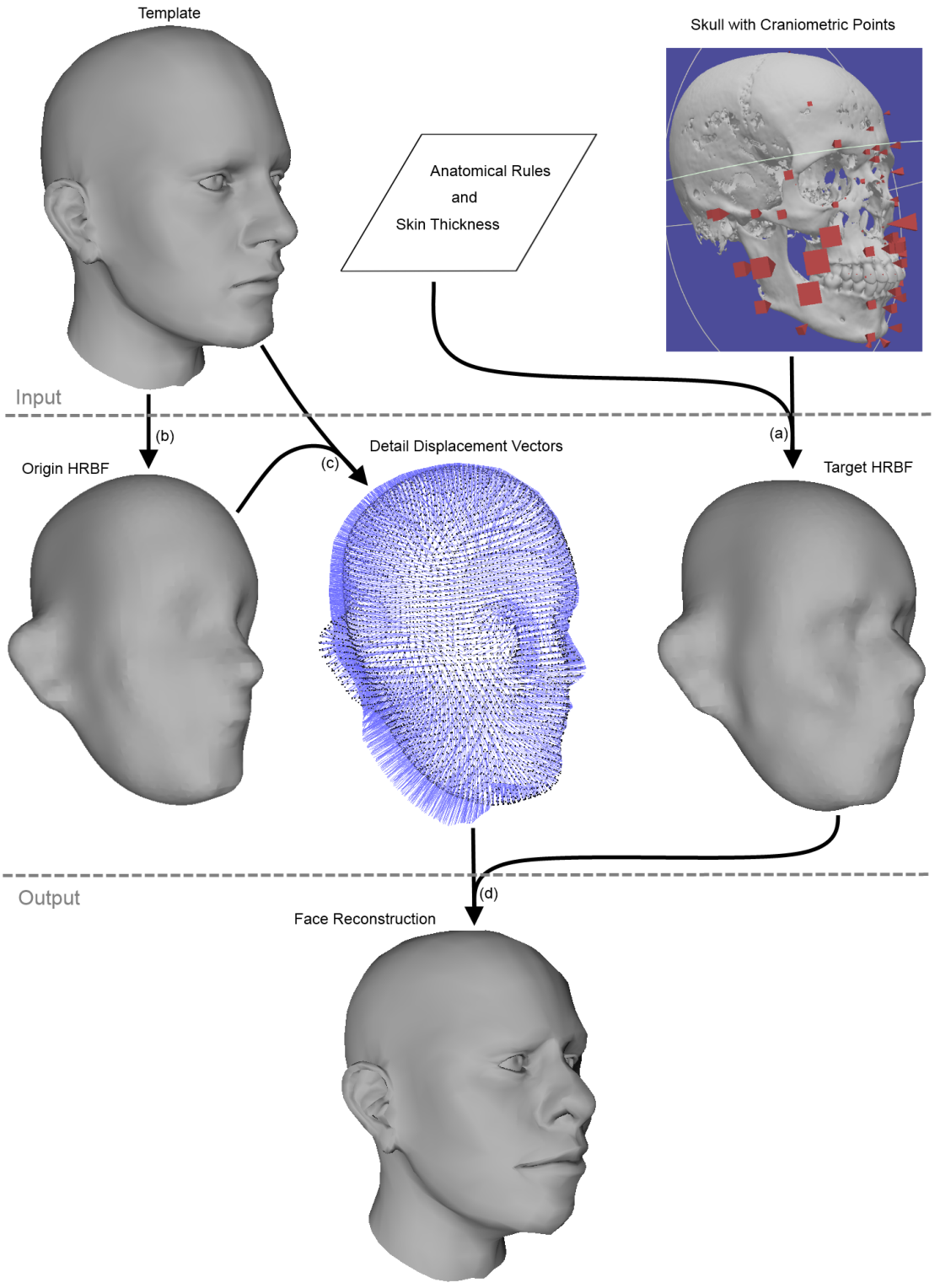

Figure 1.1: Complete workflow of our method: (a) The target HRBF is created from the craniometric points, skin thickness and anatomical rules; (b) The origin HRBF is created from the template; (c) The detail displacement vectors are created from the differences between the template and the origin HRBF; (d) The face reconstruction is obtained by adding the detail displacement vectors to the target HRBF.

Chapter 2

Related work

Computerized automation of the facial reconstruction has been previously proposed in other works. Most of these related works use craniometric points as a base for facial reconstruction, however they employ different interpolation and restriction techniques.

Pascual et al. [2] propose a method to generate a great number of intermediate points between the virtual depth markers of known thickness (analogous to those used in the manual method) through a triangulation procedure. The projection of each intermediate point on the skull is computed. Then, a new thickness and normal direction are applied to each intermediate point by interpolating the thickness and normal of the nearby craniometric points.

The result of this method is a triangular mesh without soft tissue structures like eyes, nose, ears and mouth. The lack of those structures imposes an enormous difficulty on identification. On the other hand, the results are not biased toward the shape of any reference facial template. Also, the whole topology of the skull is used to produce the surface of the face, not just a few craniometric points. This entails advantages in regions with smooth variations on the skull. However, in regions with greater variations on the skull, the replication of the skull surface at the face is not desirable.

Vanezis et al. [3] propose the use of a database of facial templates with the soft tissue points corresponding to the craniometric points marked. For an input skull, a set of templates are selected according to the skull anthropological criteria (age, gender and ethnicity). With the craniometric points marked on the input skull, the tissue depth data are used to estimate points on the face. The selected templates are then deformed so that their soft tissue points match the corresponding facial estimated points from the skull.

This deformation is done in a point-wise fashion through a three dimensional transformation termed warp. First, a Procrustes transform is done to establish the position and orientation that best fits the facial landmarks of the template to the

facial landmarks estimated from skull. Then, a set of radial-base functions (RBF) is derived to finish the warp. In this way, the templates are adapted to accommodate the skull.

Given the uncertainty of the exact shape of the soft tissue structures, Vanezis proposes the use of a police indenti-kit system to add all sort of features such as eyes, beard and hats over a two-dimensional view of the reconstructed face. Nevertheless, the soft tissue structures are not significantly modified by the proposed deformation method, biasing the results toward the database's templates and any subsequent replacement of soft tissue structure would be arbitrary.

Kahler et al. [4] also propose the deformation of a template with a RBF warp given the craniometric points restrictions. However, they include additional reconstruction hints inserting automatically interpolated landmarks on the mandible and anatomical heuristics regarding the nose and the mouth.

The width of the nose corresponds to the width of the piriform aperture at its widest point, plus 10mm. The tip of the nose lies in the extension of the nasal spine, at a distance equal to three times its length. The width of the mouth is determined by the measurement of the front six teeth. The vertical placement of the mouth corners is slightly above the blades of the incisors. The thickness of the lips can be obtained from the upper and lower incisors.

With these heuristics, the mouth and nose shapes can be better estimated as it allows to loose the assumption of orthogonal connection between corresponding skull and skin points.

At last, a virtual muscle layer is created with a mass-spring system that allows animations of facial expressions. However, the muscles are added after the facial reconstruction, and thus are not used as restrictions to model the face.

Unlike the previously described approaches, Hu et al. [5] propose a facial reconstruction method not based on predefined craniometric points and thickness. Instead, the relationship between skull and face is acquired from corresponding pair samples of template skull and template face.

Both the skull and the face samples needs to undergo the same dense registration algorithm to build a point-to-point correspondence between them. As a result, there is a set of model coefficients that defines each skull surface and the same coefficients also defines the corresponding face surface.

The facial reconstruction is done by an iterative method that adjusts the skull model coefficients so that it gradually approaches the input skull. When the coefficients converge, the same values are used as the coefficients of the face model, producing the face estimation for that input skull.

To character the local shape variety of the main soft tissue structures, local deformable models were constructed by cutting out patches from the reference skull

and face related to eyes, mouth and nose. Using hierarchically the same method of the global model, the local models are deformed and smoothly integrated with the global model with a two-step fusion procedure.

Turner et al. [6] describe another method that is not based on craniometric points and thicknesses. It relies on a CT scan database of skulls and corresponding faces. For a new questioned input skull, between 50 and 150 known skulls from the database are deformed with a warping process to approximate it. Then, the corresponding faces of the deformed skulls are also deformed with the same warping process, resulting in a set of possible faces for that skull shape.

Through a principal components analysis of all the deformed faces, it is possible to find an average face as well as a set of eigenvectors that spans the "face-space". These eigenvectors are variation vectors that have statistical significance and can be applied with different weights over the average face to reconstruct faces with a statistically quantifiable likelihood of occurring in the general population.

To solve the facial reconstruction problem, Duan et al. [7] propose a multi-linear subspace analysis approach to explore the relationship between the skull and skin in the tensor space. This is a generalized version of the linear principal components analysis (PCA).

First, the skull and face sample models have their back cut away and then are projected into two-dimensional depth images. The same process is performed in the input skull. The two-dimensional depth image of the input skull is divided into overlapped patches and projected into the skull tensor space.

Using partial least squares regression (PLSR), a skin tensor feature is estimated from the skull tensor feature in the tensor space. The operation defined to compute the skin tensor feature from the skin feature vector of the sample faces can be reversed. This way, the skin feature vector can be easily extracted from the skin tensor feature. From the skin feature vector a new two-dimensional depth image is composed and then back projected to the three-dimensional space.

Attributes such as age and body mass index (BMI) can also be taken into account by adding them into the regression model. The regression model was then trained from a database of 200 whole head CT scans on voluntary persons from China, as well as their age and BMI. Using this regression model, a new skin surface can be reconstructed from an input skull, an age and a BMI value.

Chapter 3

Craniometric points restriction

To the best of our knowledge, there is no automated method to identify the craniometric points. In fact, these points many times have no geometrical hints, and are based solely on the specialist's experience and notion of anatomy. Therefore, an expert is required to manually mark them on the virtual skull. An application was developed to display and manipulate the skull, allowing the expert to place markers over it's surface. The thickness (soft tissue depth) are manually inserted, but they could also be automatically recovered from a given table using some sort of identification for the points.

For each marked point on the skull's mesh, a smoothed normal vector is computed by averaging the normals of neighboring vertices. Combining the normal vector with the thickness of each point, a new point is defined, estimated to lie on the face's soft tissue (Figure 3.3a). This process defines the input of our method, that is, a set of points on the face corresponding to the craniometric points.

From the position of those points and their normals, an implicit surface could be readily generated using HRBF [8] for example. A brief explanation of HRBF is presented in Appendix A. Points can then be sampled from this surface for visualization or mesh reconstruction.

However, the normal direction obtained from the skull is not always in accordance with the direction in which the thickness of soft tissue have traditionally been measured and tabulated. For some points, the normal direction must be adjusted up, down, laterally or medially. Therefore, it is important to define an anatomically natural position and orientation to the skull.

The most important head anatomical planes are the Frankfurt plane, which separates the head into superior and inferior parts, the Midsagittal plane, which separates the head into left and right parts, and the Coronal plane, which separates the head into anterior and posterior parts. It is important to note that these three planes are orthogonal to each other. In order to compute them, they must be defined relative to the skull. This is accomplished by defining the Frankfurt plane

as the plane containing the left suborbital point, the left porion point and the right porion point. The Midsagittal plane is then defined as the plane orthogonal to the Frankfurt plane containing the prostion point and the bregma point. Finally, the Coronal plane is defined as the plane orthogonal to the Frankfurt plane and orthogonal to the Midsagittal plane containing the left porion point (Figure 3.1). These three planes are sufficient to define an orientation and, with their intersection point set as origin, a position to the skull.

By means of trial and error, two types of normal direction adjustment proved to be the most effective: a circular cylinder shaped adjustment and an elliptical cylinder shaped adjustment. In the circular cylinder shaped adjustment, we take the vector that goes from the origin to the craniometric point projected on the Frankfurt plane, normalize it and set it as the normal direction. In the elliptical cylinder shaped adjustment, we take the normalized bisecting vector of the vectors that goes from the focal points $(0, 0, 50)$ and $(0, 0, -50)$ to the craniometric point projected on the Frankfurt plane and set it as the normal direction. Which adjustment is applied at which point is described at the Table 3.1.

Nonetheless, without the addition of anatomical rules, the result is a very crude face without nose, ears, eyes or mouth (Figure 3.3b and Figure 3.4b), unsuitable for recognition purposes. In order to add details, the prior knowledge of how a human face looks like must be defined apart from the input skull.

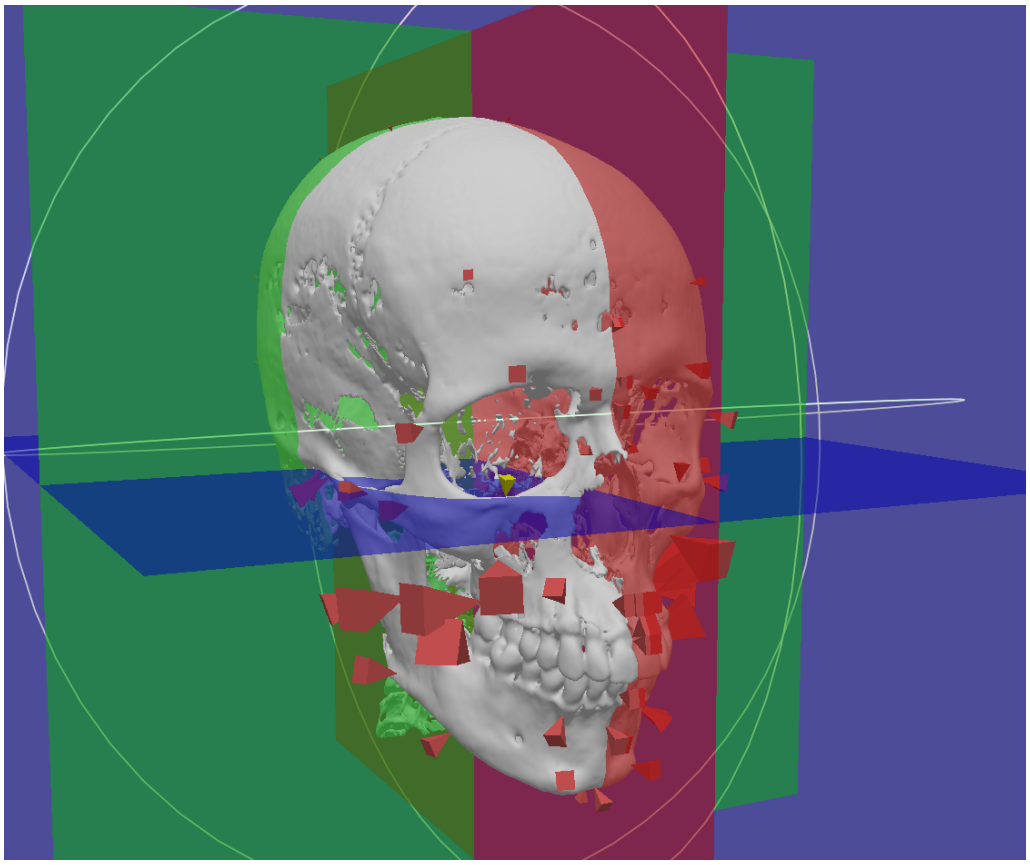

Figure 3.1: Anatomical planes: Frankfurt plane (blue), Midsagittal plane (red) and Coronal plane (green)

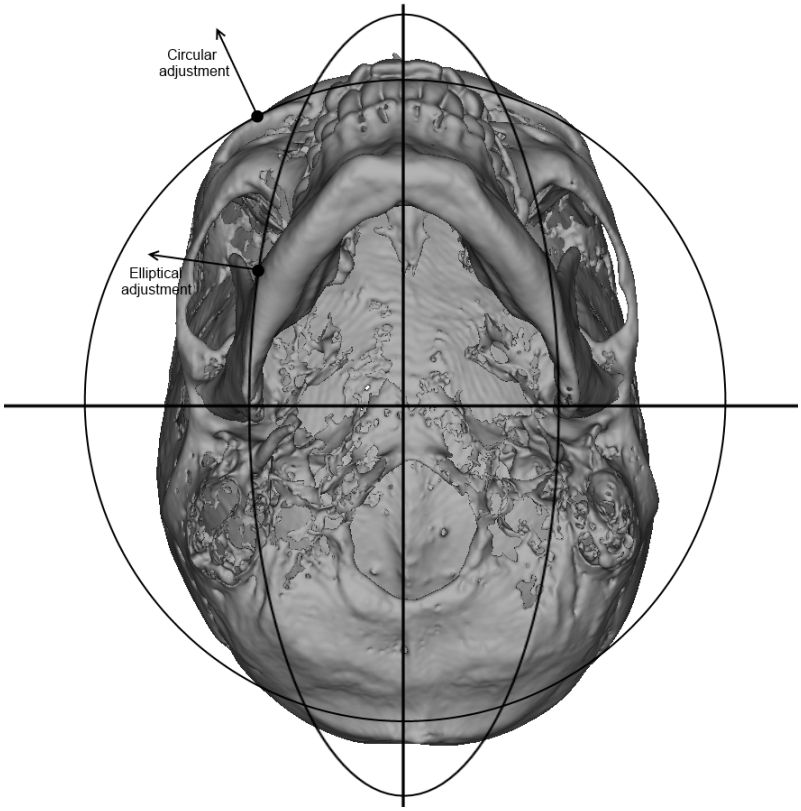

Figure 3.2: Circular and elliptical normal direction adjustments

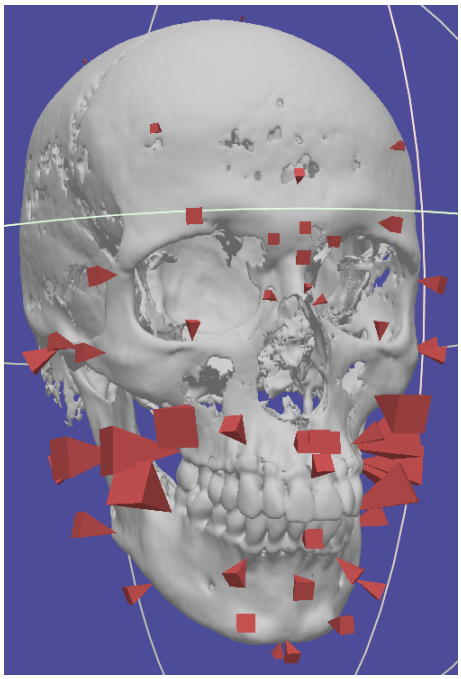

(a) Craniometric points with thickness applied in the normal direction

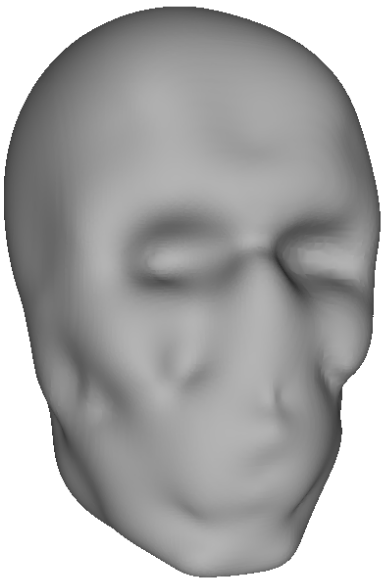

(b) Surface generated with HRBF from displaced craniometric points and normals

Figure 3.3: Craniometric points restriction

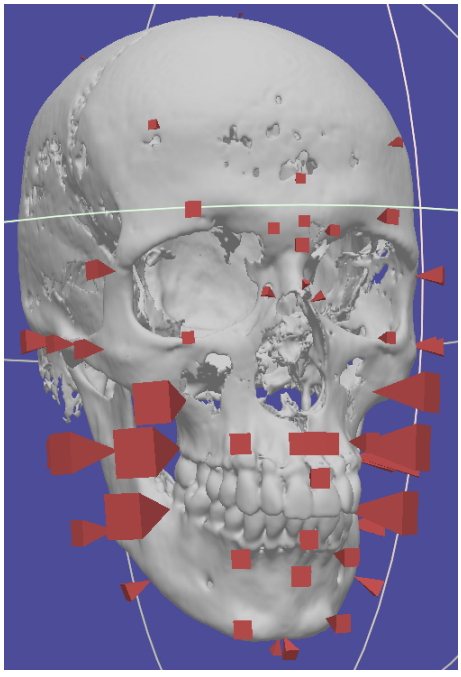

(a) Craniometric points with thickness applied in the adjusted normal direction

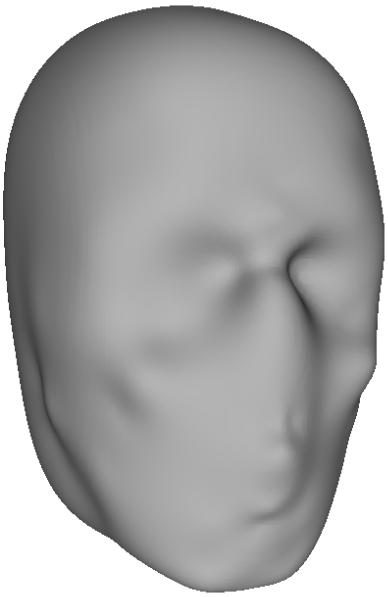

(b) Surface generated with HRBF from displaced craniometric points and adjusted normals

Figure 3.4: Craniometric points restriction with direction adjustment

Table 3.1: Summary of the skin thickness and normal direction adjustment used for craniometric points

	Point name	**Skin Thickness (mm)** * non-Brazilian values	**Normal direction adjustment**
1	Supraglabella	5.27	Elliptical
2	Glabella	6.07	Elliptical
3	Nasion	7.37	Elliptical
4	Rhinion	3.27	None
5	Prostion / Supradentale	9.72	Elliptical
6	Infradentale	9.36	Elliptical
7	Chin-lip fold / Supramentale	10.64	Elliptical
8	Gnation / Mental eminence	10.13	None
9	Subgnation / Menton	7.38	None
10	Frontal eminence (bilateral)	5.00	None
11	Supraorbital (bilateral)	8.12	Circular
12	Suborbital (bilateral)	6.35	Circular
13	Inferior malar (bilateral)	20.68	Elliptical
14	Lateral orbit (bilateral)	9.57	Elliptical
15	Zygomatic arch (bilateral)	9.45	Elliptical
16	Supraglenoid (bilateral)	13.23	Elliptical
17	Gonion (bilateral)	14.42	Elliptical
18	Supra M2 (bilateral)	24.83	Elliptical
19	Occlusal line (bilateral)	22.28	Elliptical
20	Sub M2 (bilateral)	23.26	Elliptical
21	Lateral glabella (bilateral)	5.9 *	Elliptical
22	Lateral nasal (bilateral)	4.8 *	None
23	Mid lateral orbit (bilateral)	4.7 *	Elliptical
24	Mid masseter (bilateral)	16.7 *	Elliptical
25	Supra canina (bilateral)	10.2 *	Elliptical
26	Sub canina (bilateral)	9.3 *	Elliptical
27	Mental tubercule anterior (bilateral)	9.2 *	Elliptical
28	Mid mandibular (bilateral)	9.5 *	None

Figure 3.5: Craniometric point positions in frontal view and side view.

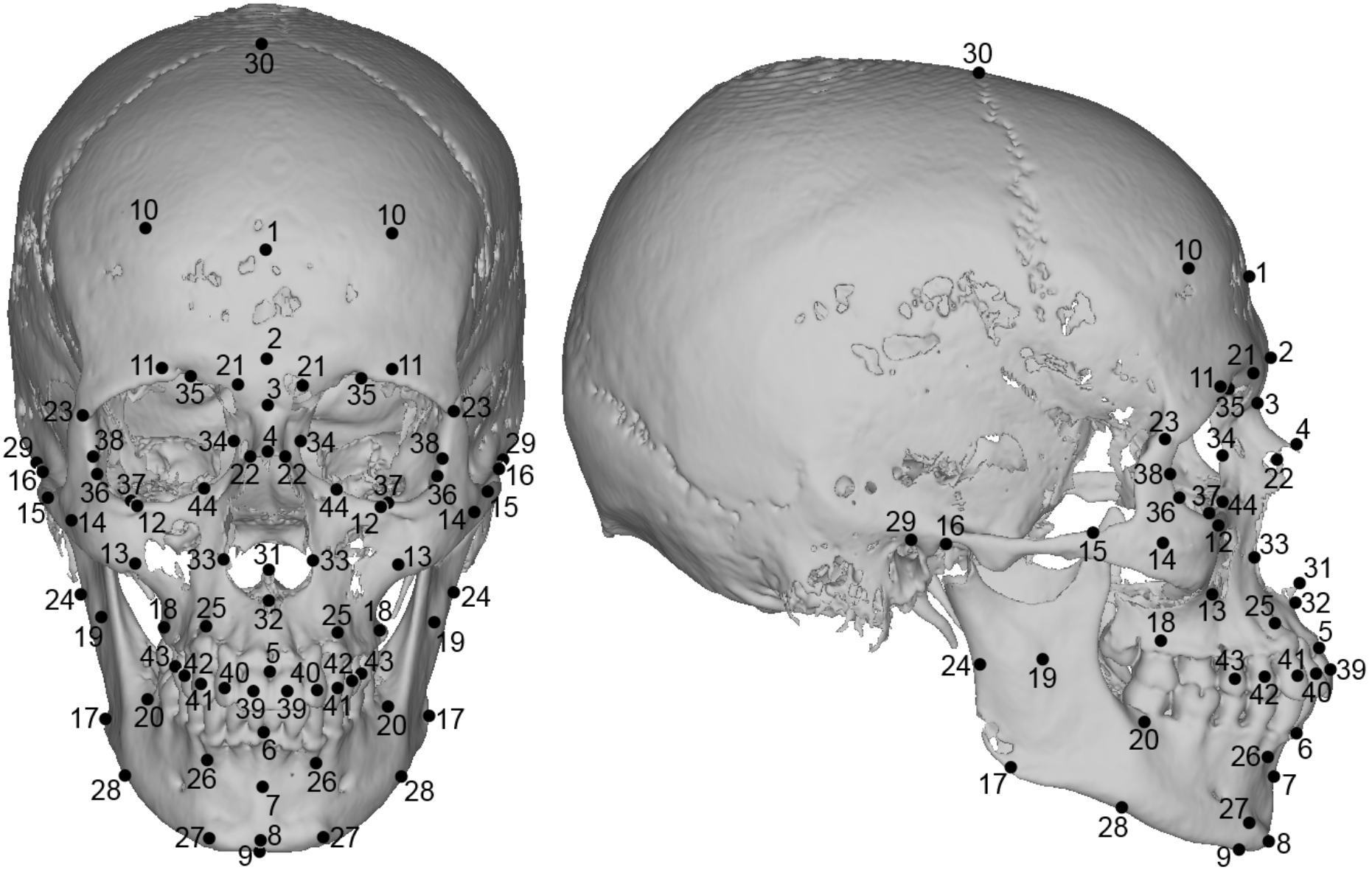

Chapter 4

Curves restriction

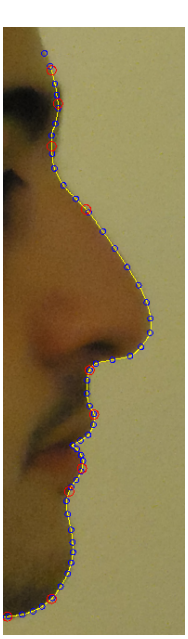

(a) Curve acquisition

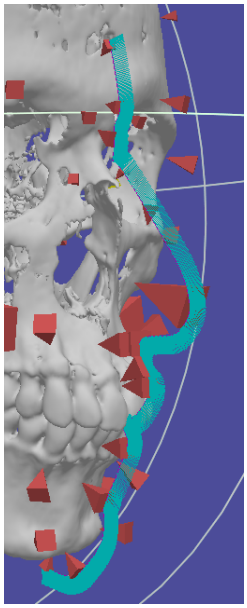

(b) Curve adaptation

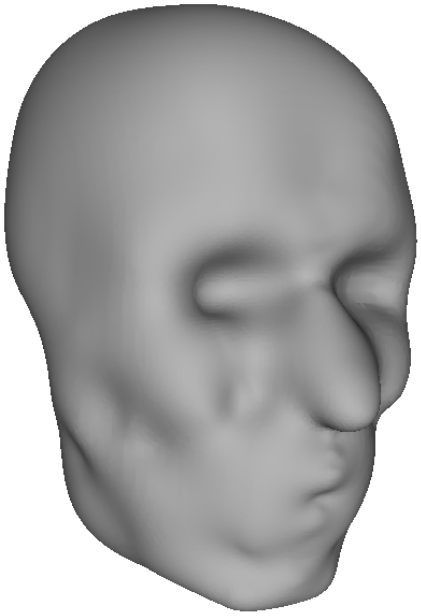

(c) Reconstruction with additional profile curve restriction

Figure 4.1: Curves restriction

A first attempt to add these missing structures was through two-dimensional curves. The curves were obtained manually from a profile image of a face, and defined as a Catmull-Rom spline [9]. The points corresponding to the craniometric points on soft tissue were marked on the image (Figure 4.1a). By matching the marked points of the curve with those already calculated from the skull, the best position and orientation of the curve in relation to the skull is retrieved. The curve is then deformed as rigidly as possible using a moving least squares approach [10] for an exact fit (Figure 4.1b).

Sample points of the adapted curve are taken and their normals evaluated. The adapted curve points are then fed to the HRBF surface generation together with the

other points from the soft tissue (Figure 4.1c). Even though it is a clear improvement from the bare HRBF reconstruction, apart from the profile curve, it is hard to define other curves over the face that are easily traceable and identified over the skull. Even more, the adapted curve seems to not provide sufficient details necessary for identification.

Chapter 5

Anatomical restrictions

To improve the quality of the result, even more anatomical knowledge must be fed to the system. However, one must be extremely cautious not to bias the result towards the features of the extra input information. In order to lessen this issue, a series of anatomical rules were surveyed from the facial reconstruction literature in order to add new restrictions computed from the input skull itself.

Most anatomical rules make reference to the anatomical planes previously mentioned (Figure 3.1).

5.1 Nose

5.1.1 Nasal profile

With the linear regressions presented by Rynn et al. [11], the pronasale position can be computed from the pronasale projection and height. Also, with the nasal height and nasal depth, the subspinale position is determined from the pronasale and nasion' (Table 5.1 and Figure 5.1).

Alternatively, the two tangent method [12] can be used to adjust the nasal tip, which showed better results in some cases (Figure 5.2).

Yet a third approach may be used to define the entire nasal profile from the shape of the piriform aperture as described by Prokopec and Ubelaker [13]. A line A is drawn passing through the nasion and prostion points. A parallel line B is then

Table 5.1: Linear regressions for the nasal profile

Pronasale projection	$0.83Y - 3.5$	All
Pronasale height	$0.9X - 2$	All
Nasal height	$0.63Z + 17$	Female
	$0.78Z + 9.5$	Male
Nasal depth	$0.5Y + 1.5$	Female
	$0.4Y + 5$	Male

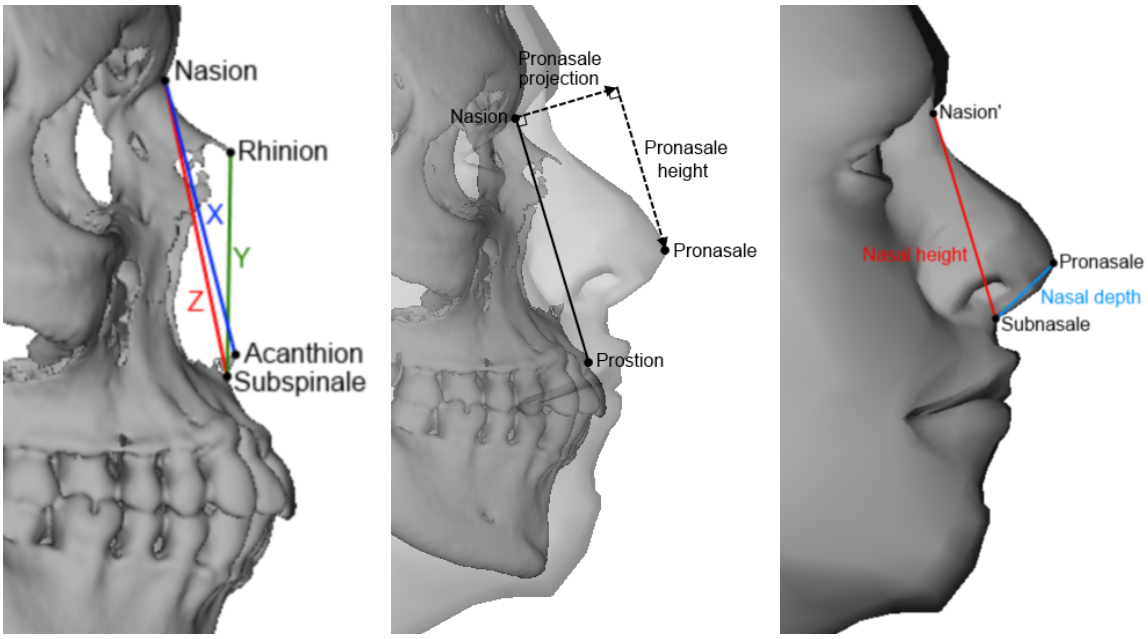

(a) X = Nasion-Acanthion distance, Y = Rhionion-Subspinale distance, Z = Nasion-Subspinale distance

(b) Pronasale position from the pronasale projection and height

(c) Subspinale position from the nasal height and depth

Figure 5.1: Pronasale and subspinale computation

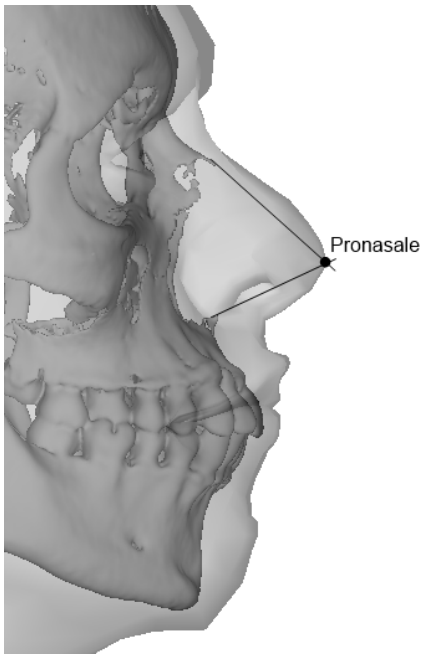

Figure 5.2: The two tangents method

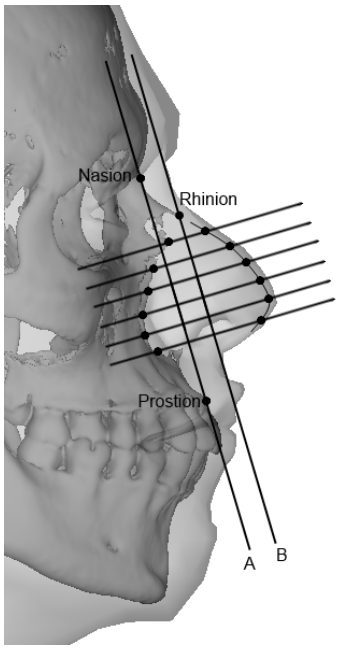

Figure 5.3: Prokopec and Ubelaker nose profile method

Table 5.2: Nasal width formulas

Hoffman et al. APF	= (PAW) +12.2	Whites
	= (PAW) +16.8	Blacks
Hoffman et al. MPF	= 1.51(PAW)	Whites
	= 1.63(PAW)	Blacks
5/3 rule	(5/3)(PAW)	All

drawn passing through the rhinion point. Then, the shape of the piriform aperture is reflected in relation to line B and increased by 2mm of skin thickness (Figure 5.3).

5.1.2 Nasal width

In conjunction with the nasal profile methods, the nasal width can be calculated from the lateral margin of the piriform aperture with either the addition prediction formulas or multiplication prediction formulas as described by Hoffman et al. [14] or the 5/3 rule [15] (Table 5.2 and Figure 5.4).

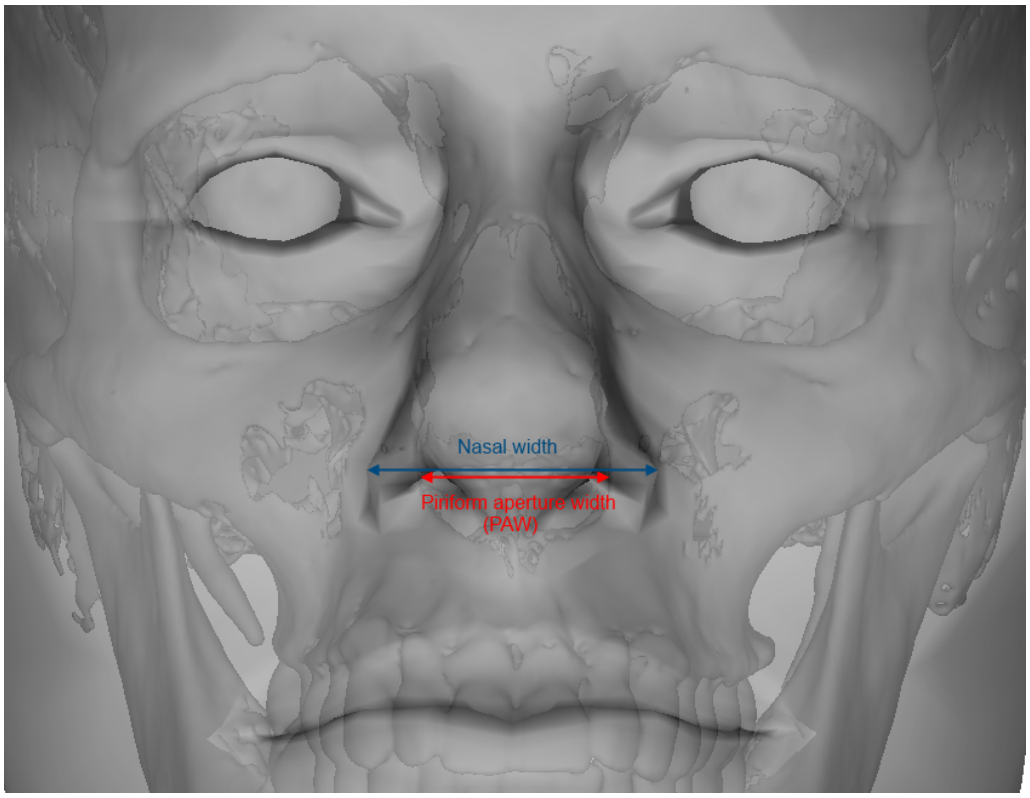

Figure 5.4: Nasal width

5.1.3 Nasal tip curve

Davy-Jow et al. [16] states that the nose tip curvature mimics the curvature of the superior portion of the nasal aperture when the head is tilted upward so that the pronasale point is superimposed over the rhinion point. We implemented a generalization of this rule by obliging the nose tip curvature to be a scaled version of the curvature of the superior portion of the nasal aperture for any specific tilt angle (which is reduced to the previous case with a scale value of one for the pronasale-rhinion superimposition). Within the scope of the generalized rule, the best results were obtained when the rhinion point was superimposed over the nasion point (Figure 5.5).

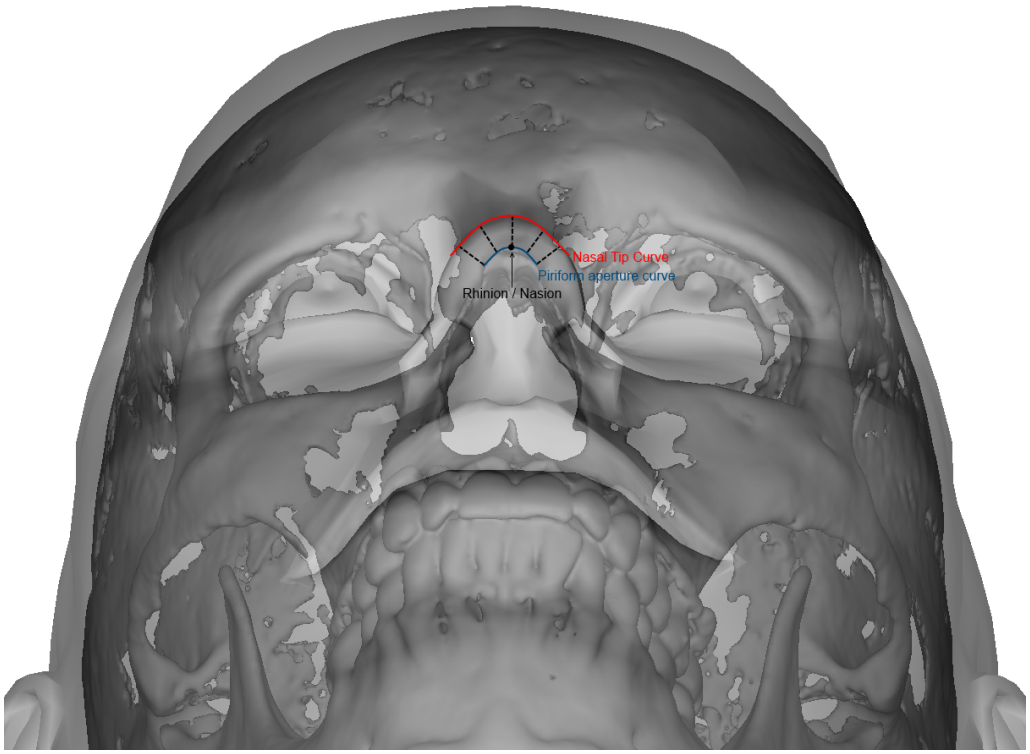

Figure 5.5: Nasal tip curve

5.2 Eyes

5.2.1 Eyeball and canthi positions

The eyeball positions as well as the canthi positions were calculated from the margins of the orbital cavity keeping the proportions of the average values given by Stephan et al. [17] [18] (Table 5.3 and Figure 5.6).

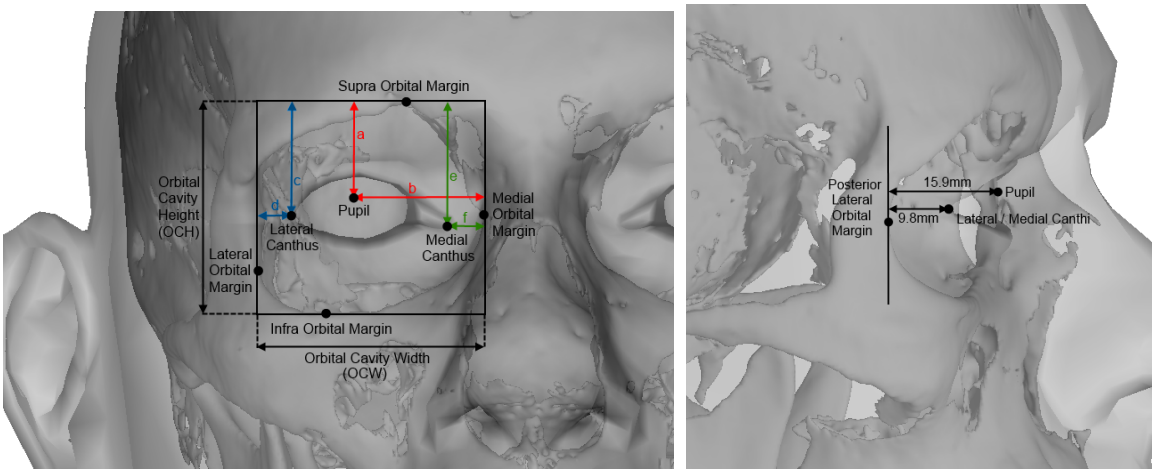

(a) Frontal view (b) Side view

Figure 5.6: Eyeball and canthi positions

Table 5.3: Eye proportions

(a)	$= 0.47(\text{OCH})$
(b)	$= 0.57(\text{OCW})$
(c)	$= 0.53(\text{OCH})$
(d)	$= 0.14(\text{OCW})$
(e)	$= 0.56(\text{OCH})$
(f)	$= 0.15(\text{OCW})$

5.2.2 Palpebral margins

The average value of the height of the palpebral fissure is 10.2mm [19], the inferior palpebral margin should touch the iris while the superior palpebral margin should cover 2mm of the iris [20]. These three restrictions can be easily met at the same time by placing the superior palpebral margin 4.1mm over the pupil and the inferior palpebral margin 6.1mm under the pupil, thus setting the iris diameter to 12.2mm, which is in the high end of its range [21] (Figure 5.7).

5.3 Mouth

5.3.1 Mouth fissure and lip thickness

For the mouth, the lip fissure was placed at a distance of the subnasal point equal to 31,2% of the distance between the subnasal and gnation points [22]. The upper and lower lip thickness can be predicted from the height of the upper and lower incisors [23] (Table 5.4, Figure 5.8 and Figure 5.9).

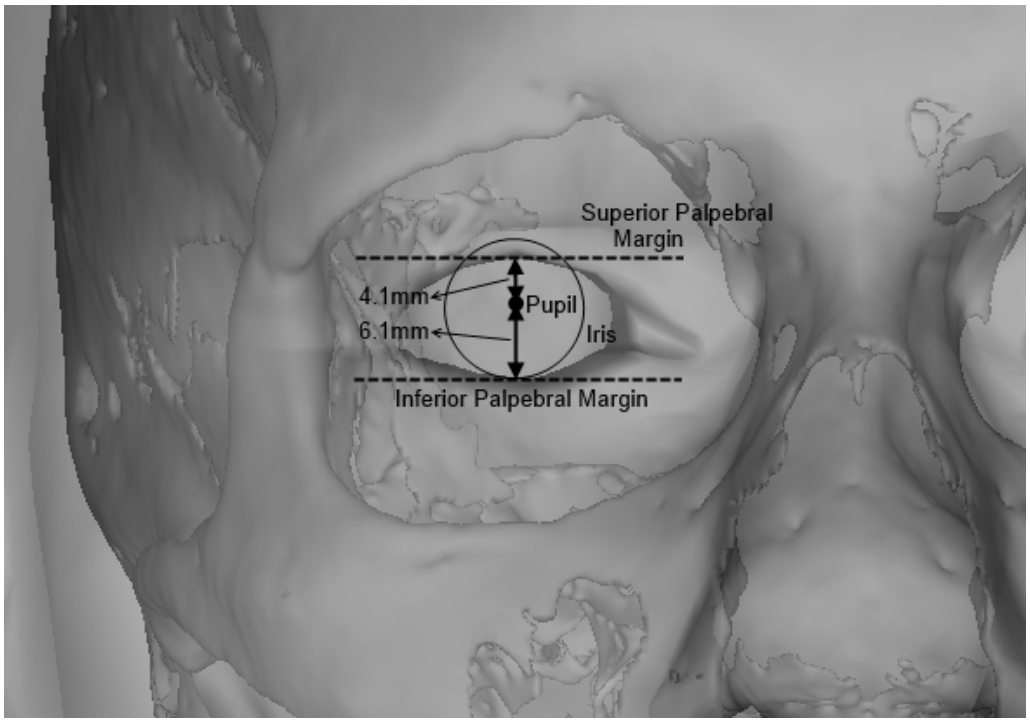

Figure 5.7: Palpebral margins

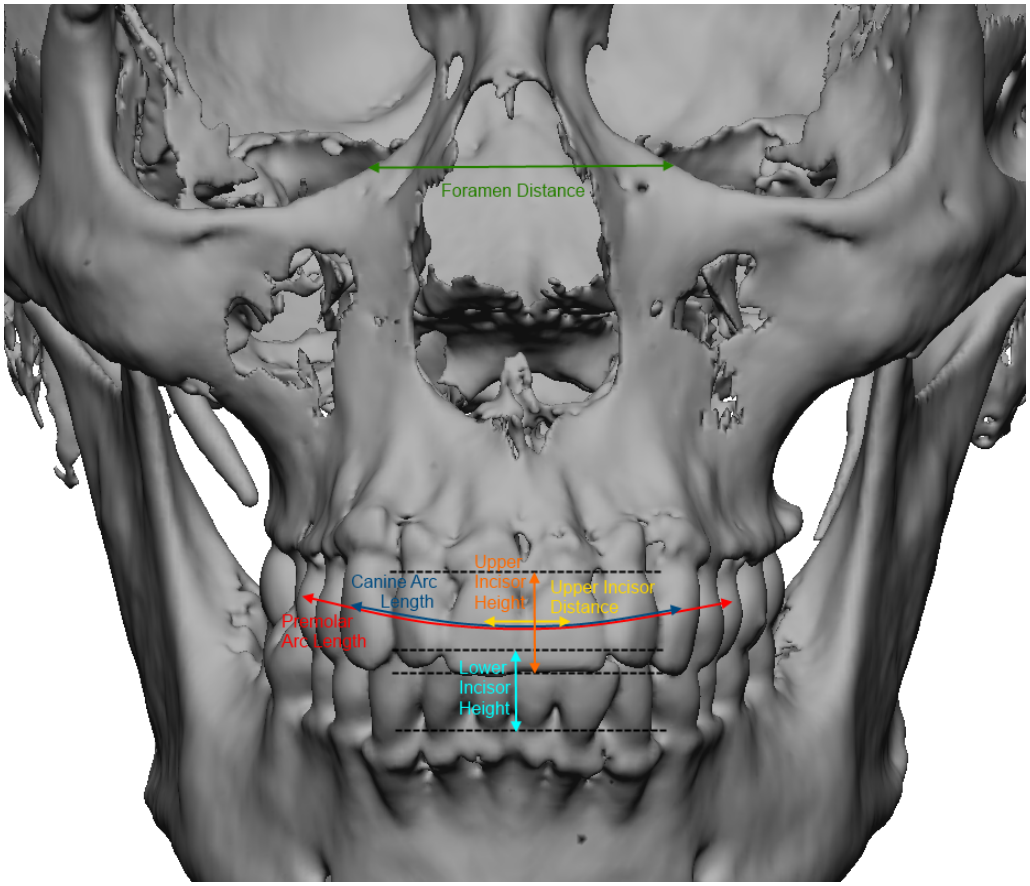

Figure 5.8: Mouth craniometric measurements

5.3.2 Mouth width

The mouth width can be obtained from formulas based on the length of the arc between the two premolars [24], on the length of the arc between the two superior canines [25] or on the distance between the two infraorbital foramen [26] (Table 5.4, Figure 5.8 and Figure 5.9).

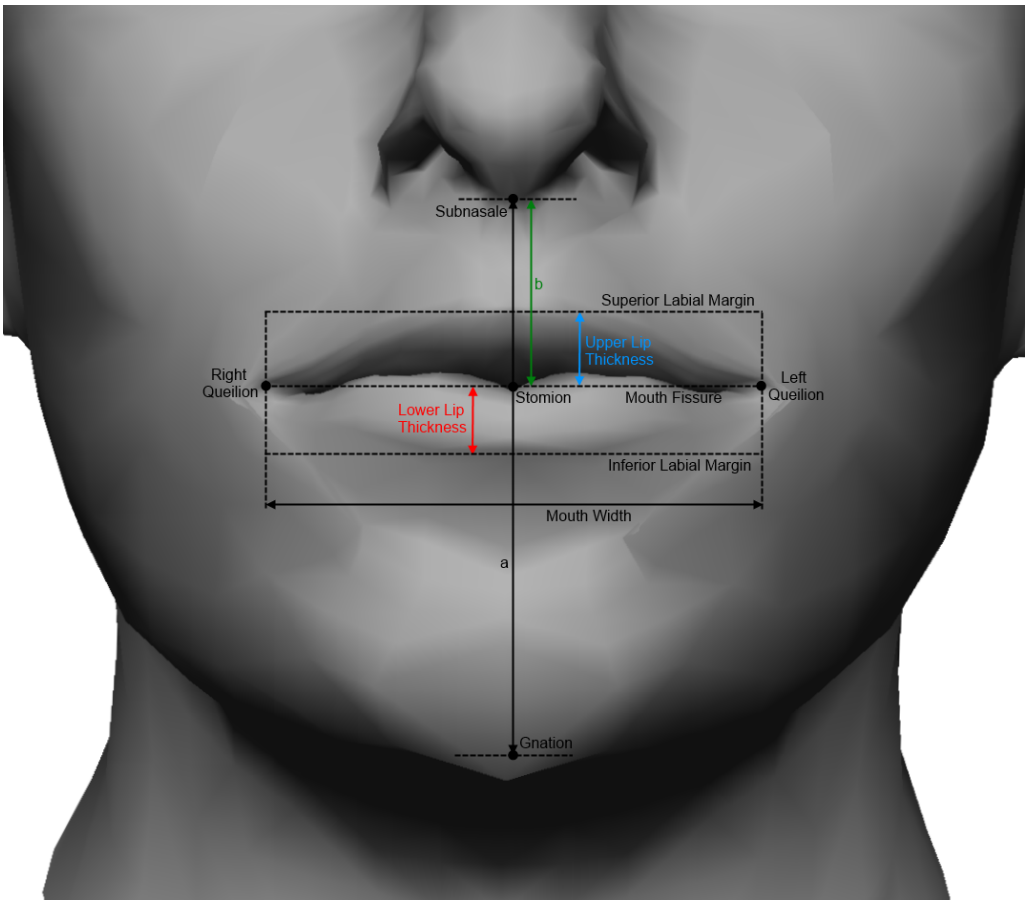

Figure 5.9: Mouth prediction

5.3.3 Cupid's bow

The cupid's bow shape can be defined from the average central bow angle [27] coupled with the width of the philtrum, which can be estimated from the distance between the central incisors [28] (Table 5.4, Figure 5.8 and Figure 5.10).

5.4 Ears

No methodological proposal was found to reconstruct the ear from the skull. Therefore, average measures for the width and length of the ear as well as the width and height of the ear lobe were used [29] (Table 5.5 and Figure 5.11).

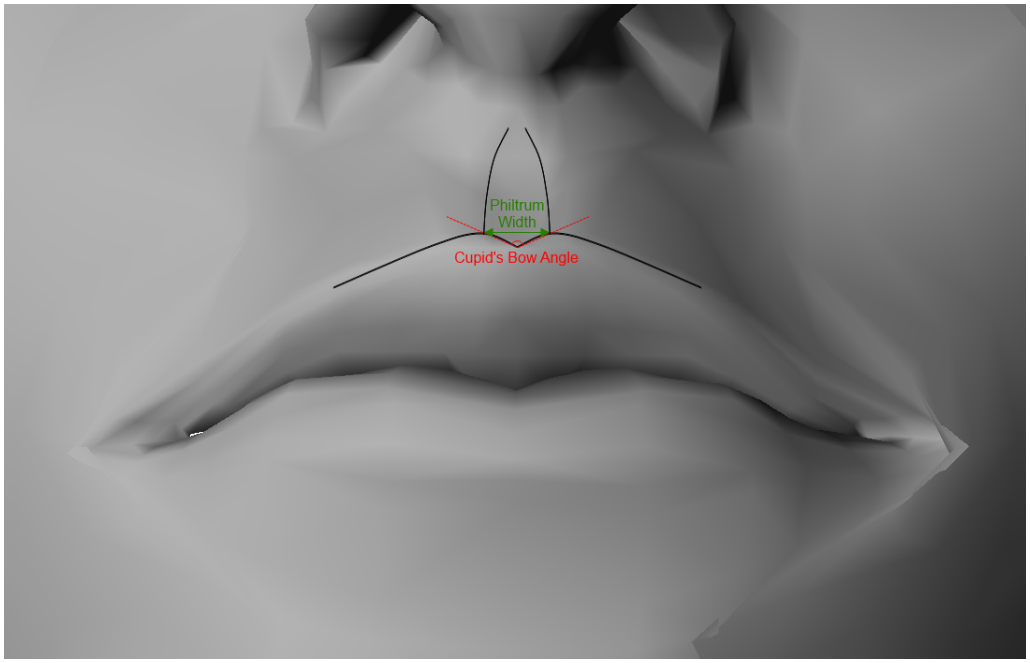

Figure 5.10: Cupid's bow

Table 5.4: Mouth formulas

(b)	$= 0.47$(a)
Upper lip thickness	$= 0.4 + 0.6$(Upper Incisor Height)
Lower lip thickness	$= 5.5 + 0.4$(Lower Incisor Height)
Mouth width	$= 21.8 + 0.7$(Premolar Arc Distance)
Mouth width	$= 0.75$(Canine Arc Distance)
Mouth width	$= 3.33$(Foramen Distance)
Philtrum width	= Upper Incisor Distance

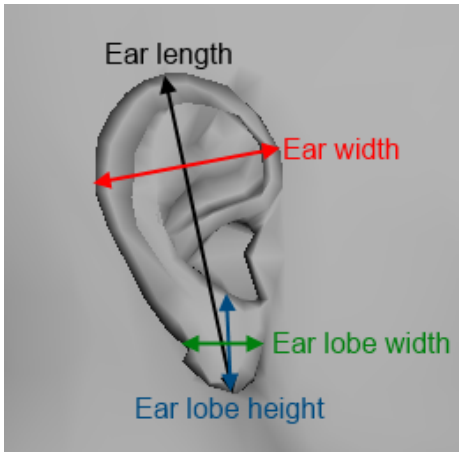

Figure 5.11: Ear measurements

Table 5.5: Ear average values

Ear width	39.99mm
Ear length	65.96mm
Ear lobe width	19.50mm
Ear lobe height	18.90mm

Table 5.6: Summary of the reconstruction options

Template	Gender	• Male • Female
	Ethnicity	• Caucasoid • Negroid • Mongoloid
Nose	Nasal Width	• 5/3 rule [15] • APF [14] • MPF [14]
	Nasal Profile	• Linear regression [11] • Two tangents [12] • Profile points [13]
	Nasal Tip Curve	• Nasal aperture curvature [16] • Generalized
Eyes	Eyeball Position	• Ocular orbit proportions [18]
	Canthi Position	• Ocular orbit proportions [17]
	Palpebral Fissure Height	• Average [19] [20]
Mouth	Lip Fissure Level	• 31.2% subnasal-gnation [22]
	Mouth Width	• Premolar distance [24] • Intercanine distance [25] • Foramen distance [26]
	Lip Thickness	• Incisor heights [23]
	Cupid's Bow Angle	• Average [27]
	Philtrum Width	• Incisors distance [28]
Ears	Ear Length	• Average [29]
	Ear Width	• Average [29]
	Ear Lobe Width	• Average [29]
	Ear Lobe Height	• Average [29]

5.5 Reconstruction configuration

To select which combination of anatomical rules will be applied, a configuration screen was created inside our application. It is also in this screen that the gender and ethnicity are set. The Table 5.6 displays a summary of the options.

Table 5.7: Summary of the craniometric points used

	Point name	**Use**
1	Supraglabella	Skin thickness
2	Glabella	Skin thickness
3	Nasion	Skin thickness, Nasal profile (Rynn et al., Prokopec et al.)
4	Rhinion	Skin thickness, Nasal tip curve, Nasal profile (Rynn et al., Prokopec et al., Two tangent)
5	Prostion / Supradentale	Skin thickness, Midsagittal plane, Nasal profile (Prokopec et al.)
6	Infradentale	Skin thickness
7	Chin-lip fold / Supramentale	Skin thickness
8	Gnation / Mental eminence	Skin thickness, Lip fissure level
9	Subgnation / Menton	Skin thickness
10	Frontal eminence (bilateral)	Skin thickness
11	Supraorbital (bilateral)	Skin thickness
12	Suborbital (bilateral)	Skin thickness, Frankfurt plane
13	Inferior malar (bilateral)	Skin thickness
14	Lateral orbit (bilateral)	Skin thickness
15	Zygomatic arch (bilateral)	Skin thickness
16	Supraglenoid (bilateral)	Skin thickness
17	Gonion (bilateral)	Skin thickness
18	Supra M2 (bilateral)	Skin thickness
19	Occlusal line (bilateral)	Skin thickness
20	Sub M2 (bilateral)	Skin thickness
21	Lateral glabella (bilateral)	Skin thickness
22	Lateral nasal (bilateral)	Skin thickness, Nasal tip curve
23	Mid lateral orbit (bilateral)	Skin thickness
24	Mid masseter (bilateral)	Skin thickness
25	Supra canina (bilateral)	Skin thickness
26	Sub canina (bilateral)	Skin thickness
27	Mental tubercule anterior (bilateral)	Skin thickness
28	Mid mandibular (bilateral)	Skin thickness
29	Porion (bilateral)	Frankfurt plane, Coronal plane
30	Bregma	Midsagittal plane
31	Acanthion / Nasospinale	Nasal profile (Rynn et al., Two tangent)
32	Subnasal / Subspinale	Nasal profile (Rynn et al.), Lip fissure level
33	Lateral piriform margin (bilateral)	Nasal width (Hoffman et al., 5/3 rule)
34	Medial orbital margin (bilateral)	Eyeball position, Canthi position
35	Supra orbital margin (bilateral)	Eyeball position, Canthi position
36	Lateral orbital margin (bilateral)	Eyeball position, Canthi position
37	Infra orbital margin (bilateral)	Eyeball position, Canthi position
38	Posterior lateral orbital margin (bilateral)	Eyeball position, Canthi position
39	Superior central incisor (bilateral)	Dental arch curvature, Philtrum width
40	Superior lateral incisor (bilateral)	Dental arch curvature
41	Superior canine (bilateral)	Dental arch curvature, Mouth width (Stephan et al.)
42	Superior first premolar (bilateral)	Dental arch curvature
43	Superior second premolar (bilateral)	Dental arch curvature, Mouth width (Lebedinskaya et al.)
44	Infraorbital foramen (bilateral)	Mouth width (Stephan et al.)

Chapter 6

Template restrictions

Even with the addition of the extra points from the anatomical restrictions, there isn't enough sampling information for a proper facial reconstruction. One alternative is to use a template mesh for each soft tissue structure (nose, ear etc...), which is placed, oriented and deformed to match the restrictions outlined above. Points and normals from the meshes are then sampled and fed to the HRBF algorithm (Figure 6.1). By adding only the necessary pieces of templates we minimize the bias towards the input structures. The downside is that by separately placing these meshes, the way that the soft tissues structures are connected to each other are not entirely respected (the eye balls with the eye lids, the eye lids with the nose, the nose with the mouth and so on). The way they are linked is important and it is difficult to geometrically specify where one structure ends and another begins.

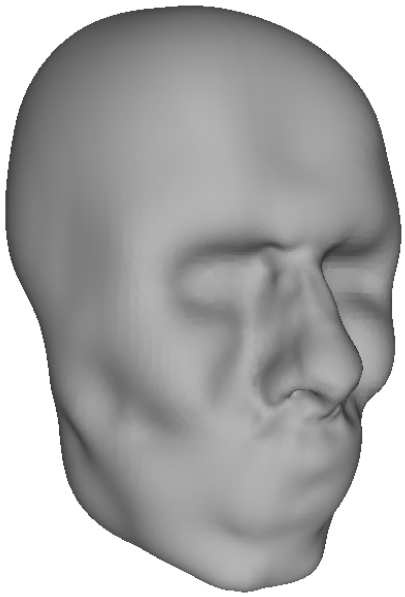

Figure 6.1: Reconstruction with nose mesh restriction

Therefore, instead of separate meshes, a full template model is employed

(Figure 7.5a, Figure 7.6a, Figure 7.7a). On one hand, by limiting the result to be a deformation of this template model, we can ensure that the result will resemble a human face. On the other hand, the risk of getting biased results is much greater. Hence, all the previous anatomical restrictions are applied and a detail transfer approach is used to guarantee that the template model will suffer enough modifications to achieved an as unbiased as possible result.

As a matter of fact, with the complete model for the face there are no gaps on the surface to be covered and the HRBF algorithm can be replaced by a simpler MLS deformation [10]. One needs only to assign the soft tissue points on the template corresponding to the craniometric points and the extra anatomical restrictions. Nonetheless, the use of MLS proved inappropriate as the deformations end up being very local, eventually introducing points of high frequency (sharp edges) and still being significantly biased towards the overall shape of the template (Figure 7.5b, Figure 7.6b, Figure 7.7b).

To restore the smoothness necessary to represent a human face and avoid biased results, a detail transfer based on the HRBF deformation is proposed. Two implicit surfaces are produced: one from the points calculated from the input skull to be the target (Figure 6.2b) and one from the corresponding points picked on the template model to be the origin (Figure 6.2a). These surfaces can be seen as basic low-frequency structures of the faces, i.e., lacking details. The details from the template model are stored as difference vectors from the HRBF surface to the points on the template mesh. These detail vectors are then transferred to the skull's HRBF surface to restore the facial restrictions (Figure 6.3). This detail transfer procedure automatically adapts the soft tissue structures to the overall shape of the input skull and preserves the template mesh topology. This process is illustrated in Figure 1.1.

To produce an HRBF surface, as opposed to an RBF surface, a normal vector must be provided for each interpolation point. To produce the origin HRBF surface, the normals of the template mesh are used, since it is a simplification of this mesh. For the target HRBF surface, ideally the subject skin normals would be used. However, this information is not available for the reconstruction. The normals of the template mesh are skin normals, but not of the subject, while the normals of the input skull are particular to the subject, but the skull normal may not be related to the skin normal depending on the region. Bearing this in mind, the skull normal was used where the skin thickness was small enough so that the skin normal was related to the skull normal (skin thickness smaller than 5 mm), otherwise, the template normal was used.

Note that the detail transfer procedure alone is not enough to achieve plausible results. Figure 8.1 shows a reconstruction with the anatomical restrictions left aside. In this case the deformation is unable to adapt the specificities of the soft tissue

structures to the skull.

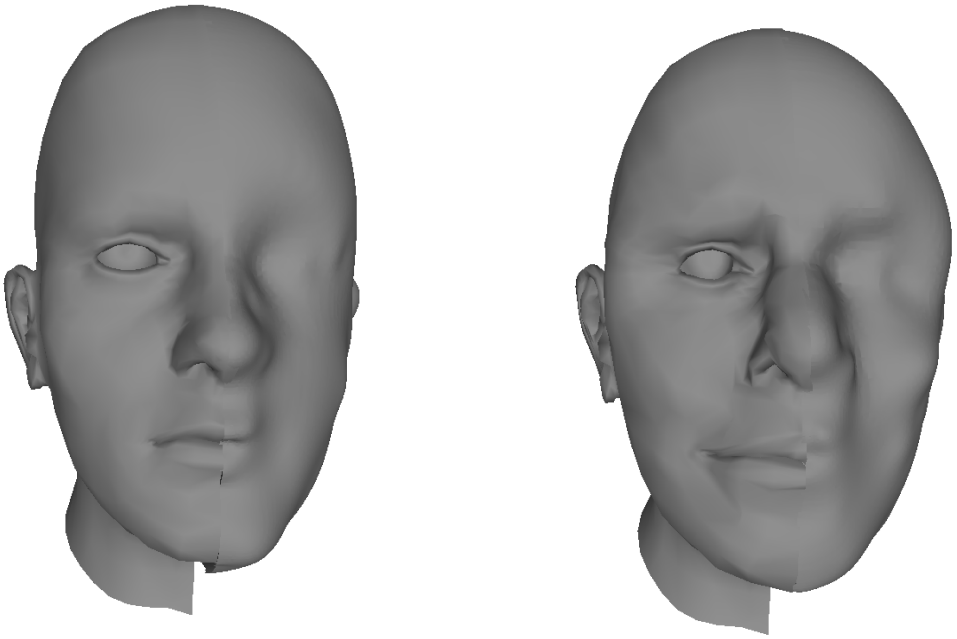

(a) Template (left) and origin HRBF from template (right)

(b) Detail transfer result (left) and target HRBF from skull (right)

Figure 6.2: HRBF face approximation for detail transfer

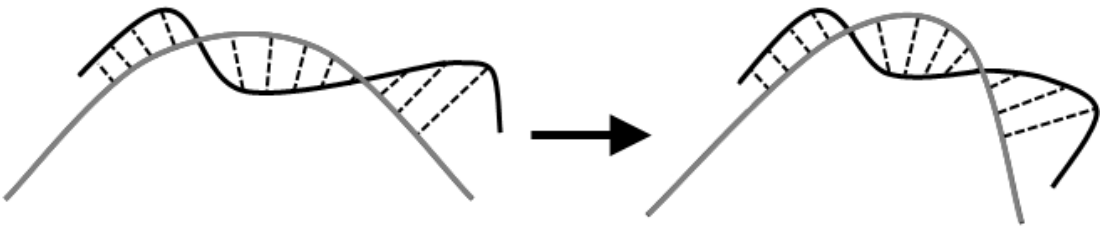

Figure 6.3: The detail (black) over the smooth HRBF surface (grey) being transferred to the other smooth HRBF surface

Chapter 7

Results

Our test subjects underwent CT scans and had their faces scanned to produce input skulls models and corresponding ground truths. With the help of a professional in the field of forensic medicine, a set of 76 craniometric points were marked for each skull. The thicknesses entered were average measures for Brazilians [30] and a few non-Brazilian measures [31]. The exact thickness values used are displayed at the Table 3.1.

The method described in this work produced very accurate results (Figure 7.5c, Figure 7.6c, Figure 7.7c) for our test subjects (Figure 7.5d, Figure 7.6d, Figure 7.7d). The accuracy of our method can be better evaluated on the comparisons of the Figure 7.10, Figure 7.11 and Figure 7.12. However, the use of a template suitable for the gender, age and ethnicity is still required. Examples of bad template usage can be seen in the Figure 7.8 and, to a greater extent, in the Figure 7.9.

Since our work allows selecting different anatomical predicting methodologies, results with different noses (Figure 7.1, Figure 7.2 and Figure 7.3) and mouths (Figure 7.4) can be easily generated.

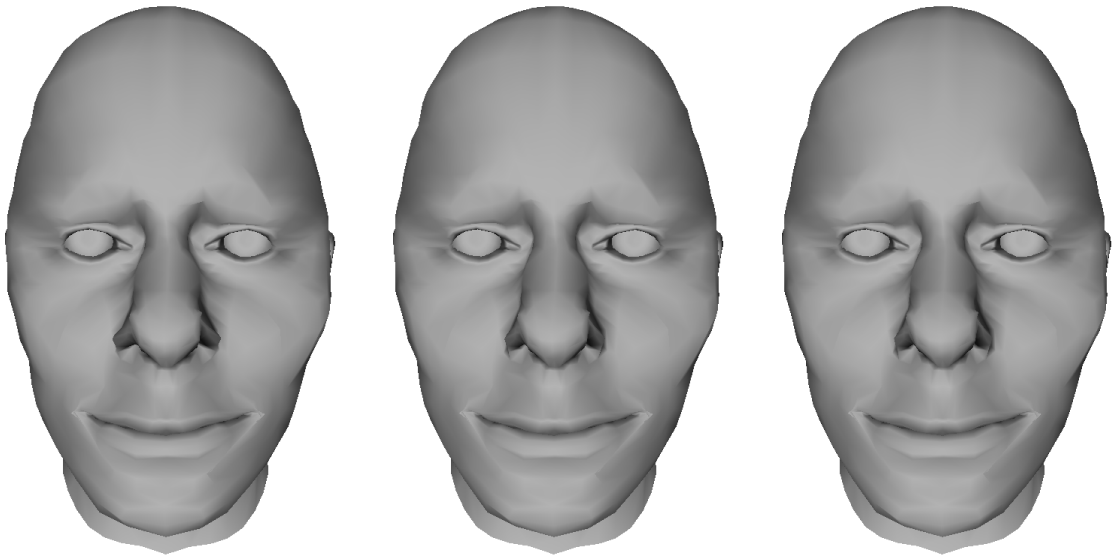

(a) 5/3 rule (b) Hoffman et al. APF (c) Hoffman et al. MPF

Figure 7.1: Different nasal width methodologies

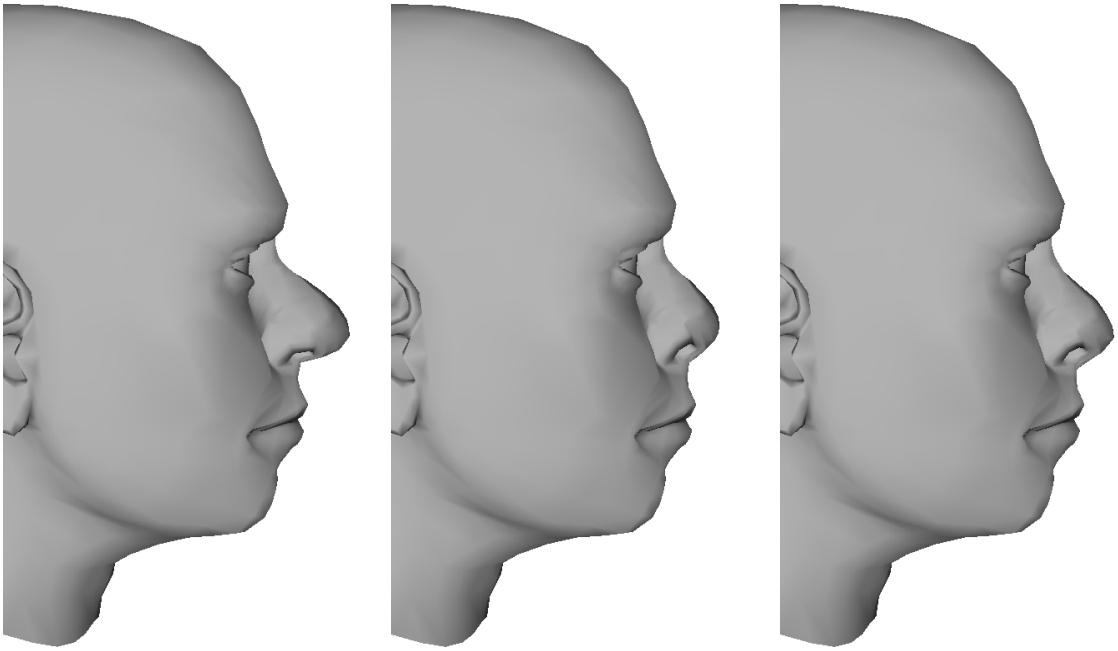

(a) Rynn et al. (b) Two tangents (c) Prokopec et al.

Figure 7.2: Different nasal profile methodologies

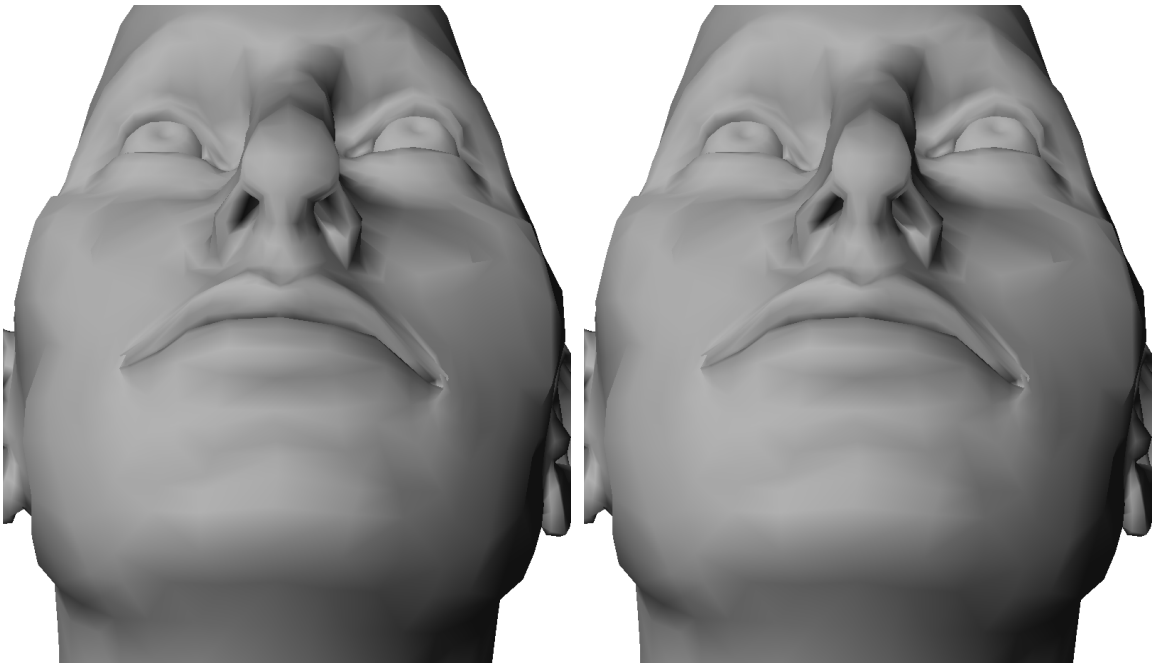

(a) Davy-Jow et al. (b) Our generalization

Figure 7.3: Different nasal tip curve methodologies

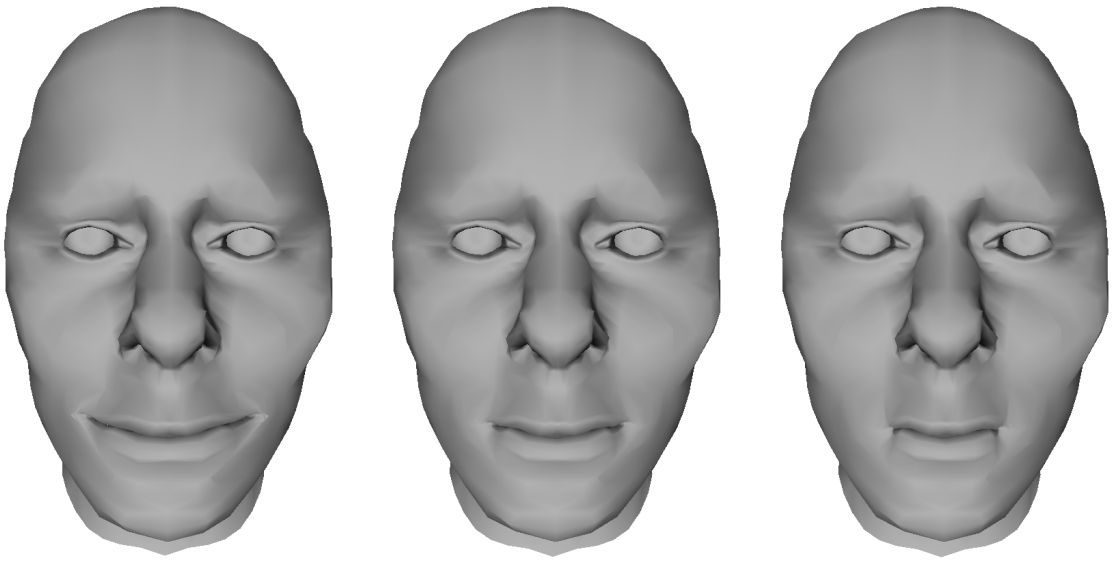

(a) Based on the premolar distance (b) Based on the canine distance (c) Based on the foramen distance

Figure 7.4: Different mouth width methodologies

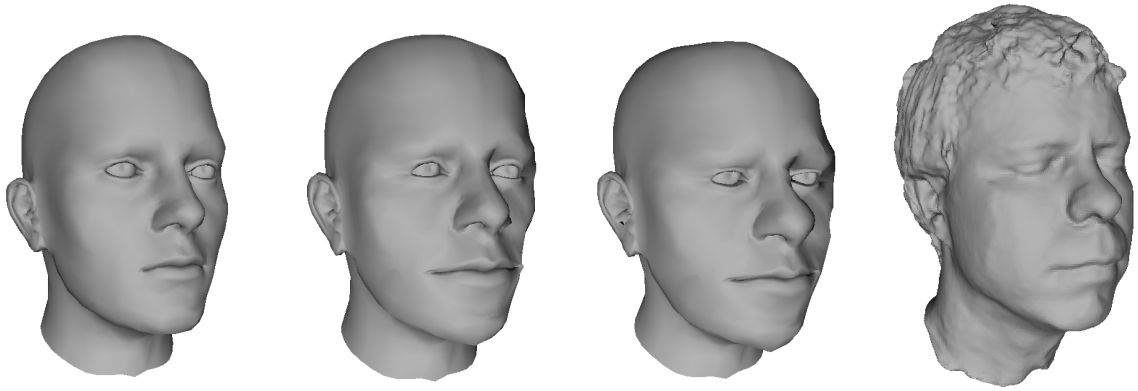

(a) Caucasoid male template

(b) Template deformed with MLS

(c) Template deformed with detail transfer over HRBF

(d) Scanned face of the caucasoid male test subject

Figure 7.5: Template, deformations and scanned face comparison for caucasoid male

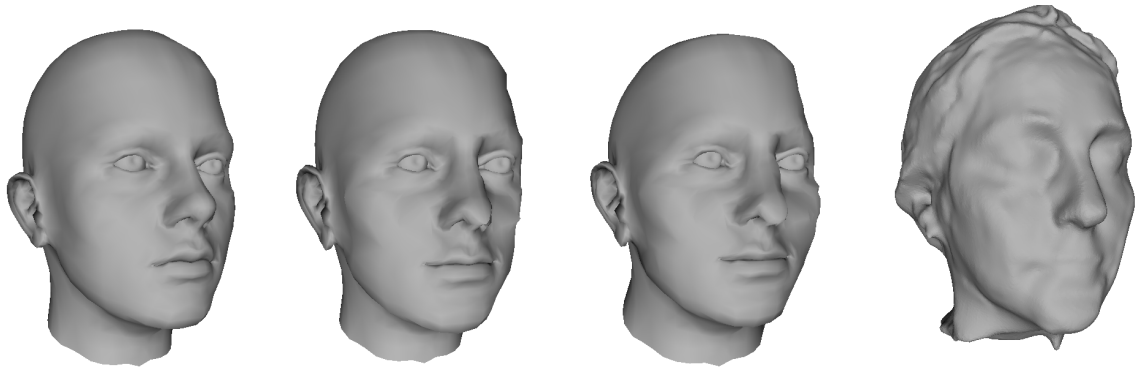

(a) Caucasoid female template

(b) Template deformed with MLS

(c) Template deformed with detail transfer over HRBF

(d) Scanned face of the caucasoid female test subject

Figure 7.6: Template, deformations and scanned face comparison for caucasoid female

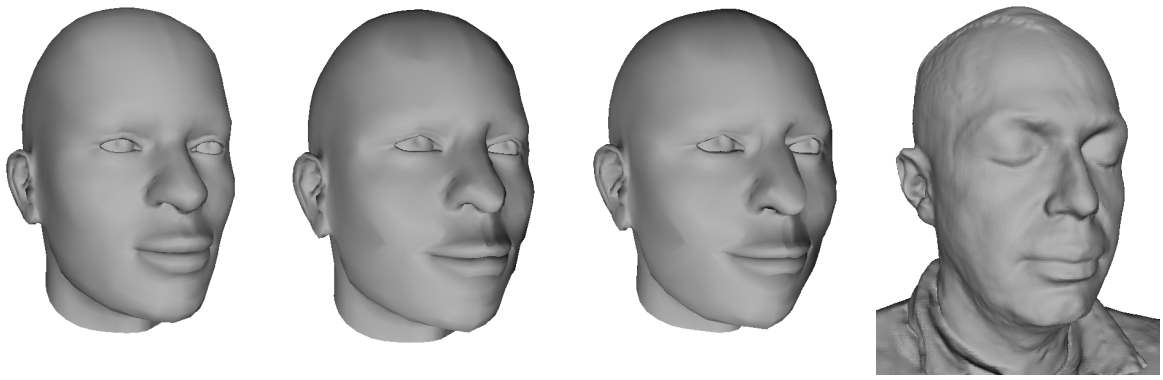

(a) Negroid male template

(b) Template deformed with MLS

(c) Template deformed with detail transfer over HRBF

(d) Scanned face of the negroid male test subject

Figure 7.7: Template, deformations and scanned face comparison for negroid male

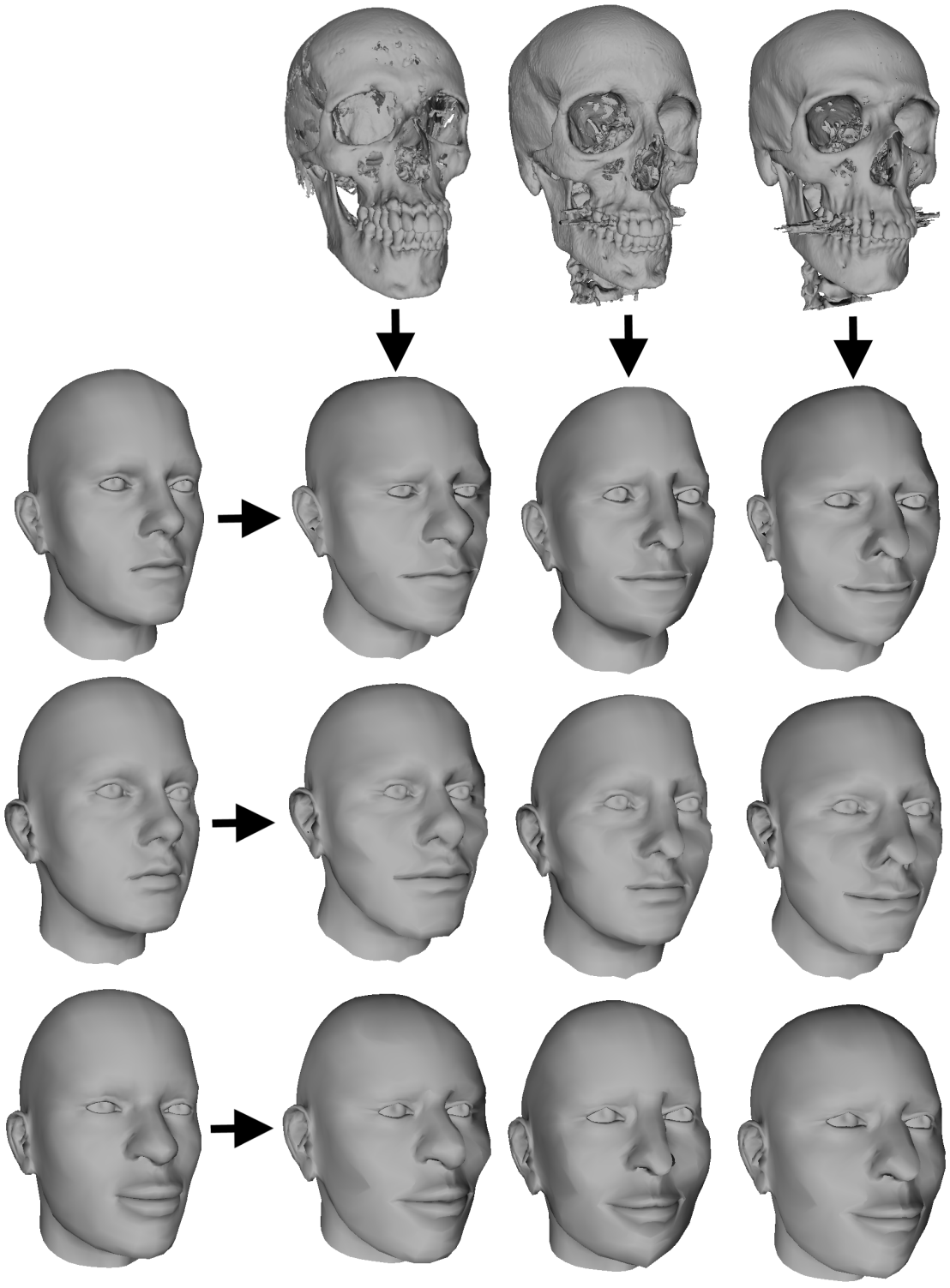

Figure 7.8: Reconstructions of all the combinations of test subject skulls and templates

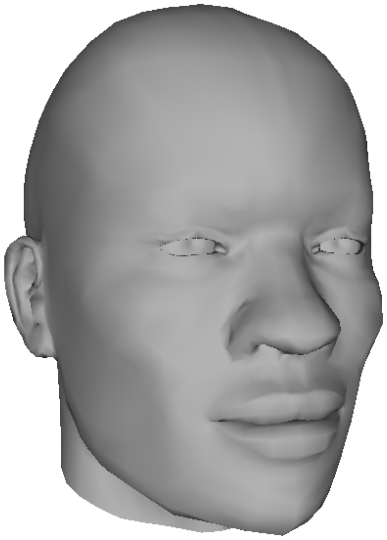

(a) An african negroid male template

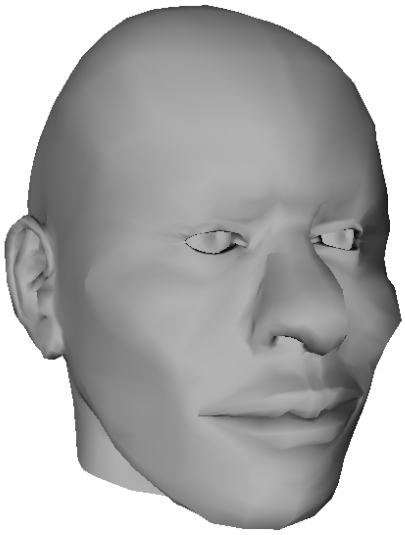

(b) Result for the caucasoid male test subject (Figure 7.5d)

Figure 7.9: Ethnicity limitation

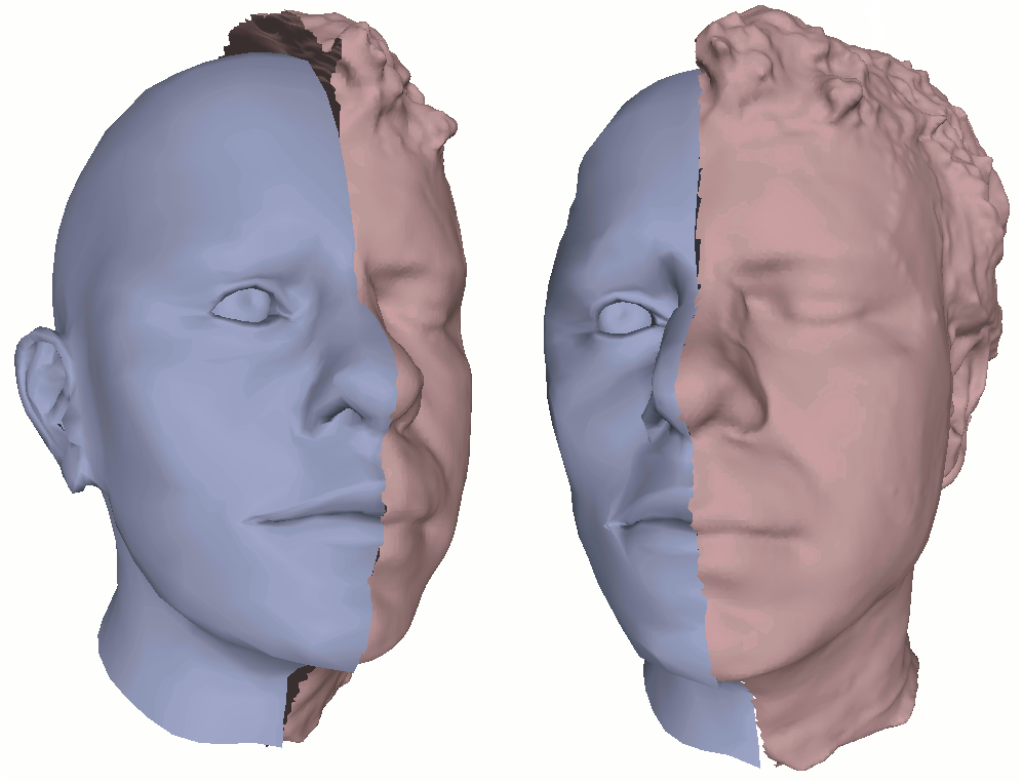

Figure 7.10: Final facial reconstruction (blue) and scanned face (red) for the caucasoid male test subject

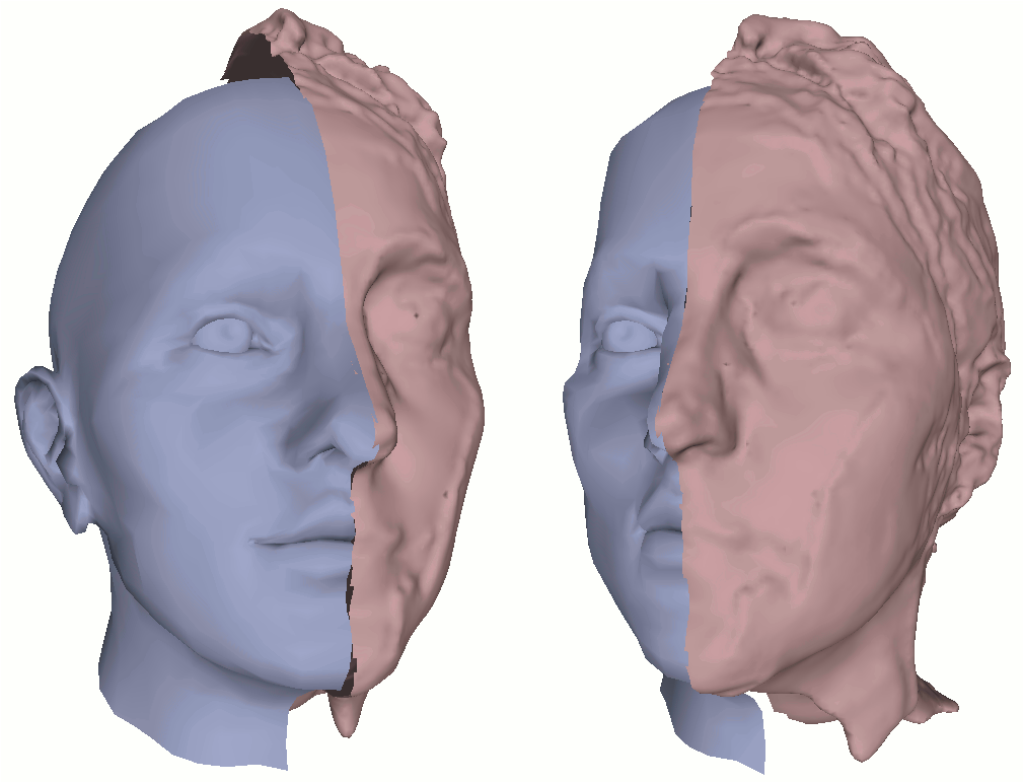

Figure 7.11: Final facial reconstruction (blue) and scanned face (red) for the caucasoid female test subject

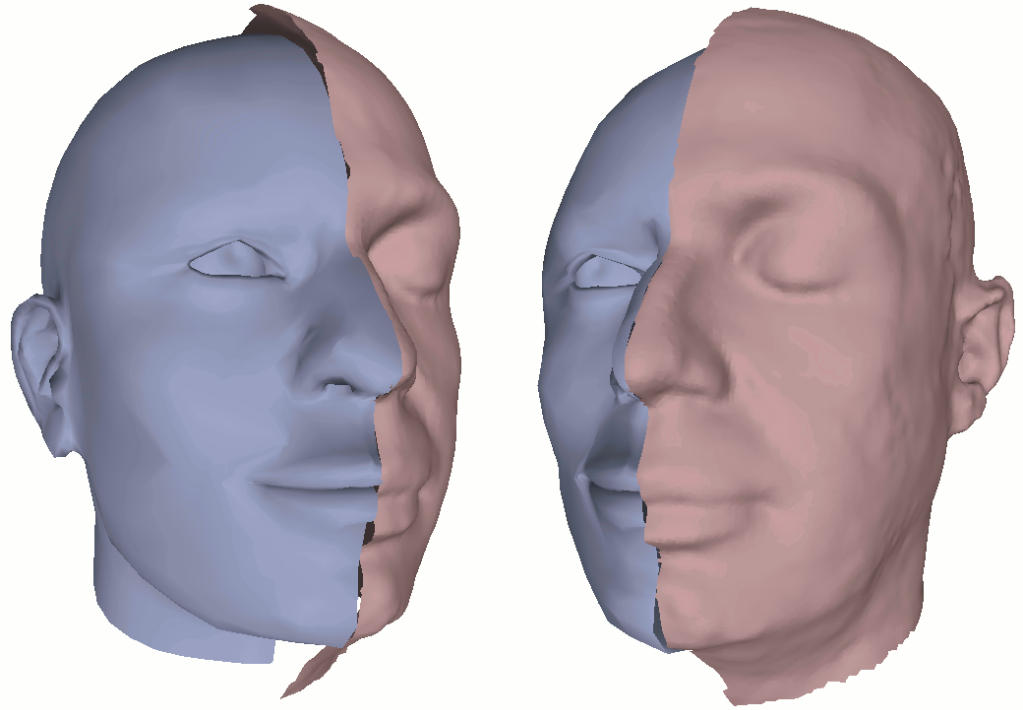

Figure 7.12: Final facial reconstruction (blue) and scanned face (red) for the negroid male test subject

Chapter 8

Conclusion and future works

In this work a wide series of anatomical rules from the facial reconstruction literature were translated into geometrical restrictions to enhance the anatomical knowledge of the system. Our novel HRBF detail transfer method for facial reconstruction provides a smooth surface while at the same time preserving the topology of the template mesh. The dissociation between detail and overall shape presented by our deformation method significantly reduces the bias towards the template.

Our first informal tests led to successful identification of the subjects. However, broader and more rigorous tests must still be conducted.

The automatic reconstruction only takes a few seconds, being a major advantage over any manual method. However, the manual placement of the craniometric points can be time consuming. Therefore, the creation of guides or computational aids for this part of the process would be a big improvement regarding its usability. In this work we only addressed the geometry of the reconstructed face and thus the visual quality of our result could be enhanced with the use of rendering techniques such as skin, hair and eye shaders. Also, new restrictions could be added to adapt the soft tissue structures of the template to the skull even further.

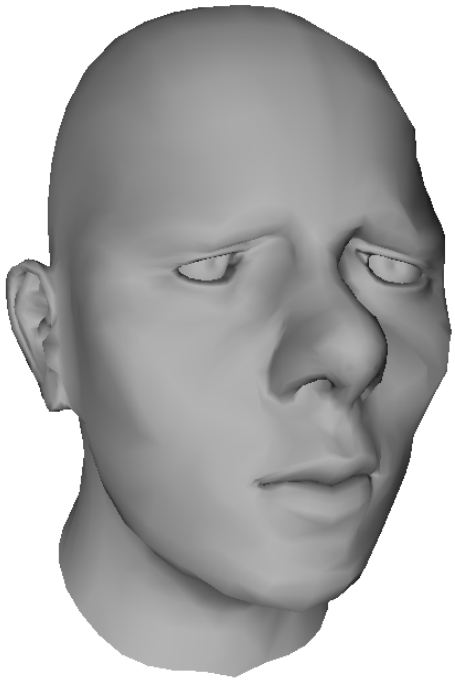

Figure 8.1: Caucasoid template (Figure 7.5a) deformed for the caucasoid male test subject (Figure 7.5d) with detail transfer over HRBF without anatomical rules. It still meets the craniometric constraints perfectly

Bibliography

[1] WILKINSON, C. "Facial reconstruction – anatomical art or artistic anatomy?" *Journal of Anatomy*, v. 216, n. 2, pp. 235–250, 2010. ISSN: 1469-7580. doi: 10.1111/j.1469-7580.2009.01182.x.

[2] PASCUAL, L., REDONDO, C., SANCHEZ, B., et al. "Computerized three-dimmensional craniofacial reconstruction from skulls based on landmarks". In: *Federated Conference on Computer Science and Information Systems (FedCSIS)*, pp. 729 –735, sept. 2011.

[3] VANEZIS, M. *Forensic facial reconstruction using 3-D computer graphics: evaluation and improvement of its reliability in identification*. Tese de Doutorado, University of Glasgow, 2008.

[4] KÄHLER, K., HABER, J., SEIDEL, H.-P. "Reanimating the Dead: Reconstruction of Expressive Faces from Skull Data", *ACM Trans. Graph.*, v. 22, n. 3, pp. 554–561, jul. 2003. ISSN: 0730-0301. doi: 10.1145/882262.882307. Disponível em: <http://doi.acm.org/10.1145/882262.882307>.

[5] HU, Y., DUAN, F., YIN, B., et al. "A hierarchical dense deformable model for 3D face reconstruction from skull", *Multimedia Tools and Applications*, v. 64, n. 2, pp. 345–364, May 2013.

[6] TURNER, W., BROWN, R., KELLIHER, T., et al. "A novel method of automated skull registration for forensic facial approximation", *Forensic science international*, v. 154, n. 2, pp. 149–158, November 2005.

[7] DUAN, F., YANG, S., HUANG, D., et al. "Craniofacial reconstruction based on multi-linear subspace analysis", *Multimedia Tools and Applications*, pp. 1–15, January 2013.

[8] MACEDO, I., GOIS, J. P., VELHO, L. "Hermite Radial Basis Functions Implicits." *Comput. Graph. Forum*, v. 30, n. 1, pp. 27–42, 2011.

[9] CATMULL, E. E., J., R. R. "A class of local interpolating splines." *Computer Aided Geometric Design*, pp. 317–326, 1974.

[10] CUNO, A., ESPERANÇA, C., OLIVEIRA, A., et al. "3D as-rigid-as-possible deformations using MLS", *In: Proceedings of the 27th Computer Graphics International Conference, Petropolis, RJ, Brazil*, p. 115–122, May 2007.

[11] RYNN, C., WILKINSON, C., PETERS, H. "Prediction of nasal morphology from the skull", *Forensic Sci Med Pathol.*, pp. 20–34, 2010.

[12] GERASIMOV. "The Reconstruction of the Face on the Skull". 1955.

[13] PROKOPEC, M., UBELAKER, D. H. "Reconstructing the Shape of the Nose According to the Skull". Paper presented at the 9th Biennial Meeting of the International Association for Craniofacial Identification, FBI, Washington, DC, July 2000.

[14] HOFFMAN, B. E., MCCONATHY, D. A., COWARD, M., et al. "Relationship Between the Piriform Aperture and Interalar Nasal Widths in Adult Males", *J. Forensic Sci.*, pp. 1152–1161, 1991.

[15] KROGMAN, W. M. *The Human Skeleton in Forensic Medicine*. Springfield, IL: Charles C Thomas, 1962.

[16] DAVY-JOW, S. L., DECKER, S. J., FORD, J. M. "A simple method of nose tip shape validation for facial approximation", *Forensic Science International*, v. 214, n. 1, pp. 208.e1–208.e3, January 2012.

[17] STEPHAN, C., DAVIDSON, P. "The placement of the human eyeball and canthi in craniofacial identification", *J. Forensic Sci.*, pp. 612–619, 2008.

[18] STEPHAN, C., HUANG, A., DAVIDSON, P. "Further evidence on the anatomical placement of the human eyeball for facial approximation and craniofacial superimposition", *J. Forensic Sci.*, pp. 267–269, 2009.

[19] KUNJUR, J., SABESAN, T., ILANKOVAN, V. "Anthropometric analysis of eyebrows and eyelids: An inter-racial study", *British Journal of Oral and Maxillofacial Surgery*, v. 44, n. 2, pp. 89–93, April 2006.

[20] CHOI, Y., EO, S. "Two-dimensional analysis of palpebral opening in blepharoptosis: visual iris-pupil complex percentage by digital photography", *Annals of plastic surgery*, v. 72, n. 4, pp. 375–380, April 2014.

[21] MASHIGE, K. P. "A review of corneal diameter, curvature and thickness values and influencing factors", *The South African Optometrist*, v. 72, n. 4, pp. 185–194, December 2013.

[22] FARKAS, L., KATIC, M., HRECZKO, T., et al. "Anthropometric proportions in the upper lip-lower lip-chin area of the lower face in young white adults", *American journal of orthodontics*, v. 86, n. 1, pp. 52–60, July 1984.

[23] WILKINSON, C., MOTWANI, M., CHIANG, E. "The relationship between the soft tissues and the skeletal detail of the mouth", *Journal of Forensic Sciences*, v. 48, n. 4, pp. 728–732, July 2003.

[24] LEBEDINSKAYA, G. V., BALUEVA, T. S., VESELOVSKAYA, E. V. "Forensic Analysis of the Skull". cap. 14, p. 183–198, Wiley-Liss, 1993.

[25] STEPHAN, C., HENNEBERG, M. "Predicting mouth width from inter-canine width - a 75rule", *Journal of Forensic Sciences*, v. 48, n. 1, pp. 725–727, July 2003.

[26] STEPHAN, C., MURPHY, S. "Mouth width prediction in craniofacial identification: cadaver tests of four recent methods, including two techniques for edentulous skulls", *The Journal of forensic odonto-stomatology*, v. 26, n. 1, pp. 2–7, June 2009.

[27] WONG, W., DAVIS, D., CAMP, M., et al. "The relationship between the soft tissues and the skeletal detail of the mouth", *Journal of plastic, reconstructive & aesthetic surgery*, v. 63, n. 12, pp. 2032–2039, February 2010.

[28] FEDOSYUTKIN, B. A., NAINYS, J. V. "Forensic Analysis of the Skull". cap. 15, p. 199–213, Wiley-Liss, 1993.

[29] SFORZA, C., GRANDI, G., BINELLI, M., et al. "Age- and sex-related changes in the normal human ear", *Forensic Science International*, v. 187, n. 1, pp. 110.e1–110.e7, May 2009.

[30] SANTOS, W. "Mensuração de tecidos moles da face de brasileiros vivos em imagens multiplanares de Ressonância Magnética Nuclear (RMN) para fins médico-legais". Thesis, Universidade de São Paulo, 2008.

[31] GREEF, S. D., CLAES, P., VANDERMEULEN, D., et al. "Large-scale in-vivo Caucasian facial soft tissue thickness database for craniofacial

reconstruction", *Forensic Science International*, v. 159, n. Supplement, pp. S126–S146, May 2006.

[32] WENDLAND, H. *Scattered Data Approximation*. Cambridge University Press, Cambridge, 2005.

[33] BACHMAN, G., NARICI, L. *Functional analysis*. Dover Publications Inc., 2000.

Appendix A

Hermitian Radial Basis Function

This appendix is a minimalist overview of Hermitian radial basis function, largely based on the work of Macêdo et al [8]. Some non-essential concepts were left aside for the sake of brevity. More in-depth explanations can be found in the aforementioned work and in the books of Wendland [32] (regarding scattered data approximation theory) and Bachman et al. [33] (regarding functional analysis).

A.1 Function approximation with RBF

A radial basis function (RBF) is a function whose value depends only on the distance to a predefined center point $\mathbf{c}$ and can be expressed as $\phi(||\mathbf{x} - \mathbf{c}||)$ or, by setting $r = ||\mathbf{x} - \mathbf{c}||$, as $\phi(r)$ from $\mathbb{R}_{\geq 0}$ to $\mathbb{R}$. The $||\cdot||$ denotes a distance function, usually the Euclidean norm.

Some examples of radial basis function are:

- $\phi(r) = r$ (linear)
- $\phi(r) = e^{-ar^2}$ (gaussian)
- $\phi(r) = \sqrt{r^2 + a^2}$ (multiquadratic)
- $\phi(r) = r^2 \ln(r)$ (thin-plate spline)

Consider a function f: $\mathbb{R}^n \to \mathbb{R}$ that we want to approximate. Given a set of points $\{\mathbf{x}_i : i = 1, 2, ..., k\}$ and their corresponding values $\{f(\mathbf{x}_i) : i = 1, 2, ..., k\}$, we can build up an approximation of the form:

$$s(\mathbf{x}) = \sum_{i=1}^{k} \alpha_i \phi(||\mathbf{x} - \mathbf{x}_i||), \qquad \mathbf{x} \in \mathbb{R}^n, \;\; \alpha_i \in \mathbb{R}$$

where the coefficients, α_i, are determined satisfying the interpolation conditions:

$$s(\mathbf{x}_i) = f(\mathbf{x}_i), \qquad i = 1, 2, ..., k$$

Since we have k variables (the weights) and k equations (the interpolation conditions), the value of the weights can be computed solving the linear system.

A.2 Surface approximation with RBF

A surface (or hypersurface on higher dimensions) can be implicitly represented by a function defined from $\mathbb{R}^n$ to $\mathbb{R}$ considering the points where its value is zero. Thus, a surface can be approximated by an implicit surface with RBF from a set of sample points $\{\mathbf{x}_i : i = 1, 2, ..., k\}$ by taking as interpolation condition $s(\mathbf{x}_i) = 0,\ i = 1, 2, ..., k$ in the mathematical framework shown before.

Sometimes, not only the position of surface sample points are available, but also the normal direction on those points. An immediate approach to take into account such information is to fabricate offset points on both sides of the surface near each sample point. The scalar values assigned to these offset points should be positive on the side indicated by the normal direction and negative on the opposite side. Even though this approach introduces some use of the normal information, it is not ideal as it does not interpolate the given normals and there is no optimal choice for the assigned scalar values.

Aligning the gradient of the approximating function with the normal direction of the sample points allows the normal restriction to be directly incorporated in the problem formulation. Formally, from a set of sample points $\{\mathbf{x}_i : i = 1, 2, ..., k\}$ and corresponding normal directions $\{\mathbf{n}_i : i = 1, 2, ..., k\}$ we want a function f: $\mathbb{R}^n \to \mathbb{R}$ that simultaneously satisfies $f(\mathbf{x}_i) = 0$ and $\nabla f(\mathbf{x}_i) = \mathbf{n}_i$ for each i = 1, 2, ..., k.

In approximation theory, this problem is known as a first-order Hermite interpolation.

A.3 Functional analysis

Before we discuss the first-order Hermite interpolation, it is important to set some fundamental theory of functional analysis.

Functional - A functional is a function whose argument is also a function. For example, the functional $\delta_{\mathbf{x}}(f) := f(\mathbf{x})$ is the evaluation functional at the point $\mathbf{x}$.

Hilbert space - A real Hilbert space $\mathcal{H}$ is a vector space equipped with an inner product $\langle \cdot, \cdot \rangle_{\mathcal{H}} : \mathcal{H} \times \mathcal{H} \to \mathbb{R}$ and that is also complete (is a Cauchy space) under

the distance function induced by this inner product.

Dual space - The dual space $\mathcal{H}^*$ of a real Hilbert space $\mathcal{H}$ is the space of continuous linear functionals $\lambda : \mathcal{H} \to \mathbb{R}$.

Generalized interpolant - Consider a set of measurement functionals $\{\lambda_i \in \mathcal{H}^* : i = 1, 2, ..., k\}$ and corresponding scalar values $\{c_i \in \mathbb{R} : i = 1, 2, ..., k\}$. A function $f \in \mathcal{H}$ is considered a generalized interpolant if $\lambda_i(f) = c_i$ for each $i = 1, 2, ..., k$.

Riesz theorem - For each $\lambda_i \in \mathcal{H}^*$ there is a unique $\upsilon_i \in \mathcal{H}$ (known as a Riesz representer) where $\lambda_i(f) = \langle \upsilon_i, f \rangle_{\mathcal{H}}$ for each $f \in \mathcal{H}$.

Minimum generalized interpolant - The unique minimum $\mathcal{H}$-norm generalized interpolant $f_{min} \in \mathcal{H}$ is a linear combination of the Riesz representers. Formally, $f_{min} = \sum_{i=1}^{k} \alpha_i \upsilon_i$ where $\alpha_i \in \mathbb{R}$ for each $i = 1, 2, ..., k$. These coefficients can be determined using the interpolation conditions $\lambda_i(f_{min}) = c_i$ to build a linear system $\mathbf{A}\alpha = \mathbf{c}$ where $A_{ij} = \lambda_i(\upsilon_j) = \langle \upsilon_i, \upsilon_j \rangle_{\mathcal{H}}$ and then solving the system.

A.4 First-order Hermite interpolation with RBF

First, we need to convert the sample points $\mathbf{x}_i$ and normal directions $\mathbf{n}_i$ into functional interpolation conditions. From the sample points we take the evaluation functional $\delta_{\mathbf{x}_i}$ over each sample point associated with the scalar value 0. From the normal directions we take the evaluation over each partial derivative associated with the corresponding component in the normal vector. Therefore, in $\mathbb{R}^3$, for each pair of sample point and normal we have the following functional interpolation conditions:

$$\lambda_i(f) = \delta_{\mathbf{x}_i}(f) = 0$$

$$\lambda_{i,x}(f) = \delta_{\mathbf{x}_i} \circ \frac{\partial}{\partial x}(f) = (\mathbf{n}_i)_x$$

$$\lambda_{i,y}(f) = \delta_{\mathbf{x}_i} \circ \frac{\partial}{\partial y}(f) = (\mathbf{n}_i)_y$$

$$\lambda_{i,z}(f) = \delta_{\mathbf{x}_i} \circ \frac{\partial}{\partial z}(f) = (\mathbf{n}_i)_z$$

In summary, all we need now to solve this problem through functional analysis is to construct a Hilbert space $\mathcal{H}$ in which the above functionals are continuous and

linearly independent. Also, it would be good if it was easy to compute their Riesz representers and the inner products among them.

If we consider every positive definite radial basis function $\phi : \mathbb{R}_{\geq 0} \to \mathbb{R}$ such that $\Psi := \phi(||\cdot||) \in C^2(\mathbb{R}^3) \cap L^1(\mathbb{R}^3)$, there is a native Hilbert space $\mathcal{H}_\phi \subset C(\mathbb{R}^3)$. In this particular space, the functionals previously presented are continuous and, provided that they are pairwise distinct, they are also linearly independent. Furthermore, their Riesz representers are, respectively:

$$\upsilon_i = \Psi(\cdot - \mathbf{x})$$

$$\upsilon_{i,x} = -\frac{\partial}{\partial x}\Psi(\cdot - \mathbf{x})$$

$$\upsilon_{i,y} = -\frac{\partial}{\partial y}\Psi(\cdot - \mathbf{x})$$

$$\upsilon_{i,z} = -\frac{\partial}{\partial z}\Psi(\cdot - \mathbf{x})$$

That yields the minimum generalized interpolant:

$$f_{min}(\mathbf{x}) = \sum_{i=1}^{k}\{\alpha_i\upsilon_i + \alpha_{i,x}\upsilon_{i,x} + \alpha_{i,y}\upsilon_{i,y} + \alpha_{i,z}\upsilon_{i,z}\} =$$

$$= \sum_{i=1}^{k}\{\alpha_i\Psi(\mathbf{x} - \mathbf{x}_i) - \alpha_{i,x}\frac{\partial}{\partial x}\Psi(\mathbf{x} - \mathbf{x}_i) - \alpha_{i,y}\frac{\partial}{\partial y}\Psi(\mathbf{x} - \mathbf{x}_i) - \alpha_{i,z}\frac{\partial}{\partial z}\Psi(\mathbf{x} - \mathbf{x}_i)\}$$

Lets set $\boldsymbol{\beta}_i = (\alpha_{i,x}, \alpha_{i,y}, \alpha_{i,z})$ so that the minimum generalized interpolant can be rewritten more compactly:

$$f_{min}(\mathbf{x}) = \sum_{i=1}^{k}\{\alpha_i\Psi(\mathbf{x} - \mathbf{x}_i) - \langle\boldsymbol{\beta}_i, \nabla\Psi(\mathbf{x} - \mathbf{x}_i)\rangle_{\mathbb{R}^3}\}$$

Finally, the scalar coefficients α_i and the vector coefficients $\boldsymbol{\beta}_i$ can be uniquely determined by the interpolation constraints $f_{min}(\mathbf{x}_i) = 0$ and $\nabla f_{min}(\mathbf{x}_i) = \mathbf{n}_i$ for each $i = 1, 2, ..., k$:

$$f_{min}(\mathbf{x}_i) = \sum_{j=1}^{k}\{\alpha_j\Psi(\mathbf{x}_i - \mathbf{x}_j) - \langle\boldsymbol{\beta}_j, \nabla\Psi(\mathbf{x}_i - \mathbf{x}_j)\rangle_{\mathbb{R}^3}\} = 0$$

$$\nabla f_{min}(\mathbf{x}_i) = \sum_{j=1}^{k}\{\alpha_j\nabla\Psi(\mathbf{x}_i - \mathbf{x}_j) - H\Psi(\mathbf{x}_i - \mathbf{x}_j)\boldsymbol{\beta}_j\} = \mathbf{n}_i$$

Where H is the hessian matrix composed of the second-order partial derivatives.